Mass Spectrometric Analysis of the Reactivity of the Trityl Cation

by

Alan An Jung Wei
B.Sc., McGill University, 2017

A Thesis Submitted in Partial Fulfillment
of the Requirements for the Degree of

MASTER OF SCIENCE

in the Department of Chemistry

Supervisory Committee

Mass Spectrometric Analysis of the Reactivity of the Trityl Cation

by

Alan An Jung Wei
B.Sc., McGill University, 2017

Supervisory Committee

Dr. J. Scott McIndoe, Department of Chemistry
Supervisor

Dr. Chris Gill, Department of Chemistry
Departmental Member

Abstract

Supervisory Committee
Dr. J. Scott McIndoe, Department of Chemistry
Supervisor
Dr. Chris Gill, Department of Chemistry
Departmental Member

Ever since its accidental discovery in the 70s, methylaluminoxane, MAO, has been a popular and widely used activator in olefin polymerization. Hydrolysis of trimethylaluminum, Me_3Al, produces MAO, an aluminum-, oxygen-, and methyl-containing oligomer. Polyolefins have become one of the most produced polymers, where MAO-activated single-site catalysts are responsible for the synthesis of polymers with highly defined structures.

The detailed structure of MAO however, remains a mystery. In order to thoroughly understand the reactivity of MAO, knowing more about it is essential. Electrospray ionization mass spectrometry (ESI-MS) has proven to be a useful technique for studying catalysts and their activation chemistry. It has been shown that MAO is best thought of as a source for the highly reactive and Lewis acidic dimethylaluminum cation, $[Me_2Al]^+$. Synthetically, this ion is accessible via the reaction between trityl tetrakis(pentafluorophenyl)borate, $[Ph_3C]^+[B(C_6F_5)_4]^-$ and trimethylaluminum, and this reaction was investigated in detail. A new reaction, substitution of H for CH_3 onto the phenyl ring of the trityl carbocation, $[Ph_3C]^+$, was detected and found to be general for all trialkylaluminums studied.

All instruments with detectors are prone to signal saturation at high concentration and mass spectrometers are no exception. Despite the advantages that ESI-MS offers,

saturation can be one of the main obstacles in terms of the accurate quantification of species.

This thesis tackles saturation issues in ESI-MS explicitly, because relatively high concentrations were necessary in order to keep unwanted decomposition reactions to a minimum. By detuning various parameters that allows troubleshooting this issue, data that better reflects the reality and the corresponding quantification of species is obtained. With the optimal settings of parameters, quantitative studies and the reactivity regarding the addition of trimethylaluminum, Me_3Al, to the trityl carbocation $[Ph_3C]^+$ can be better understood.

Table of Contents

List of Tables

List of Figures

List of Schemes

List of Abbreviations

ESI	Electrospray Ionization
ESI-MS	Electrospray Ionization Mass Spectrometry
ESI-MS (+)	Electrospray Ionization Mass Spectrometry in positive ion mode
MAO	Methyaluminoxane
MCP	Microchannel Plate
MS	Mass Spectrometry/Mass Spectrometric
MS/MS	Tandem Mass Spectrometry
m/z	Mass to charge ratio
OMTS	Octamethyltrisiloxane
PTFE	Polytetrafluoroethylene
QTOF	Quadrupole Time of Flight
TOF	Time of Flight

Acknowledgments

Firstly, I would like to thank Dr. J. Scott McIndoe. Thank you for your support, your patience, and your guidance. Thank you for giving me this opportunity and thank you for re-directing me while I was struggling.

I would also like to thank my group members and many friends who have helped me. A special thanks to Kaitlyn and Anuj. Thank you for being such great friends and helping me throughout my time in Victoria.

Finally, I would not be there without my family. Mom and Dad, thank you for the endless support. Your words of encouragement have helped me immensely.

Dedication

To Mom, Dad, and my sister.

Chapter 1 – Background

1.1 – Electrospray Ionization Mass Spectrometry (ESI-MS)

The instrument used in this work was a Micromass quadrupole time of flight (QTOF) mass spectrometer (Figure 1.1). Ions are first ionized via an electrospray ionization source, where they first pass through a quadrupole, followed by the time of flight mass analyzer then eventually reach the microchannel plate (MCP) detector.

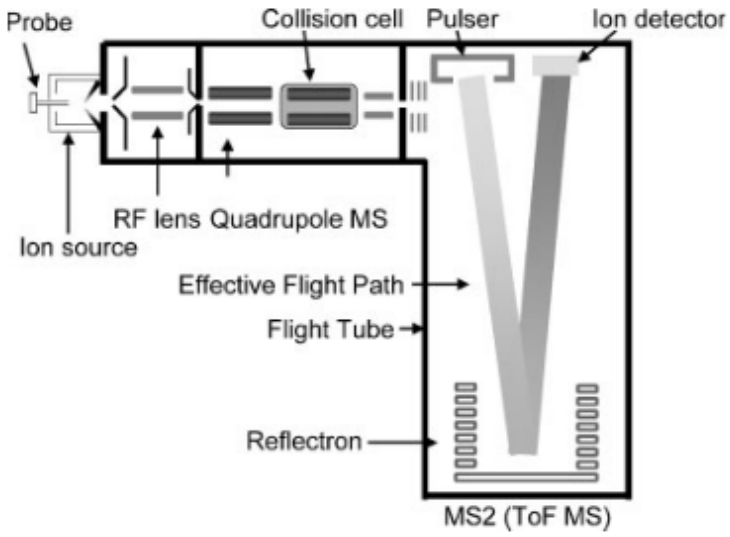

Figure 1.1 – Components of a QTOF Mass Spectrometer. Image adapted from Lacorte and reprint permission granted by John Wiley and Sons.[1]

The generation of gas phase ions with the electrospray ionization source and the sorting of ions according to their mass to charge ratio, *m/z*, will be discussed in detail to allow a better understanding of the operation of the instrument.

1.2 – Ionization

Electrospray ionization (ESI) is a soft ionization method for mass spectrometry developed in the 80s by Yamashita and Fenn.[2] It offers a sensitive and accurate analytical method for transferring solution-phase ions to the gas phase in order to determine their *m/z* ratio.[3]

Through a charged metal capillary, typically set up to 3000 V, a solution that contains the analyte is introduced with a syringe pump via PTFE tubing with a controlled flow rate in direct sample infusion. With a stream of heated inert gas, nitrogen is the one used for this instrument, and with an elevated temperature, normally set higher than the boiling point of the solvent of choice, evaporates the solution. The evaporation of solvent[4] leads to droplet shrinkage causing an increase in the electric field normal to the surface of droplets. When the repulsion between the charges increases and overcomes the surface tension at the droplet surface, ion evaporation takes place.[5] A cone jet that can be seen at the capillary tip is generated, this is known as the Taylor cone.[6] Repeated ion evaporations occur, and a continuous spray is generated (Figure 1.2).

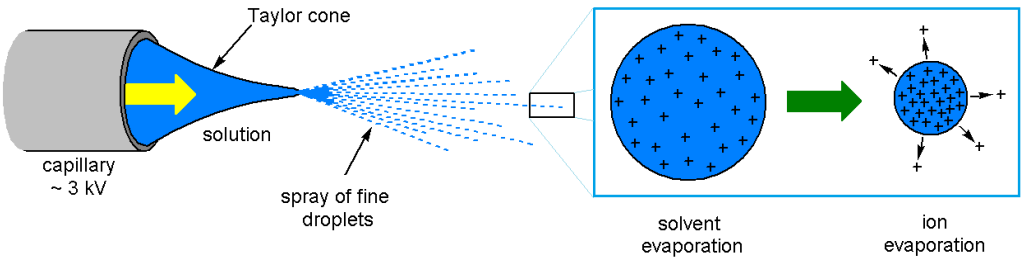

Figure 1.2 – Electrospray Ionization (ESI) source.

With the advantages of being able to separate and analyze both positively and negatively charged species (Figure 1.3), ESI-MS is a powerful tool to analyze organometallic complexes and large biomolecules.[7]

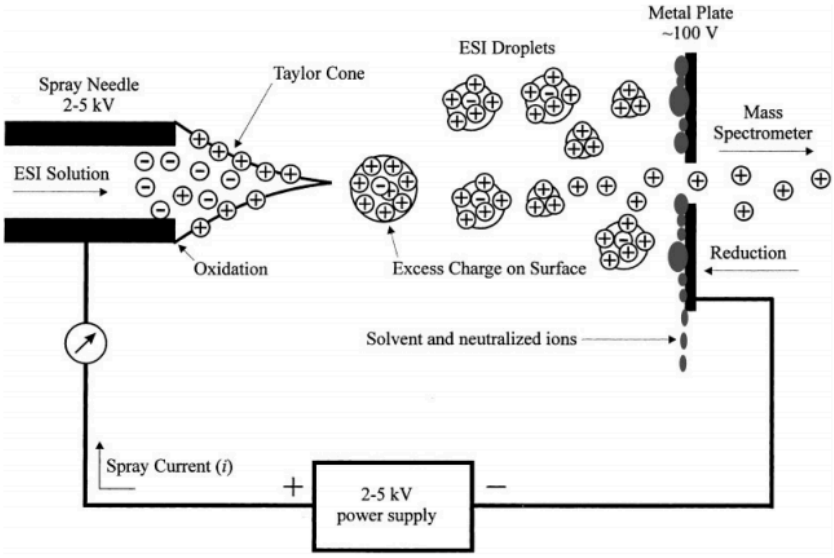

Figure 1.3 – Schematic of the electrospray ionization process. Image adapted from Cech and reprint permission granted by John Wiley and Sons.[8]

Despite the advantages that ESI-MS offers for quantitative studies, limitations such as the saturated condition can pose a problem in terms of the accurate quantification. The capillary voltage setting is crucial for the quality of the spray that is also responsible for the sensitivity. By lowering the capillary voltage, the ionization efficiency can be affected, affecting the generation of the gas phase ions.[9] The distance between the capillary tip and the orifice leading into the mass spectrometer can be tuned in some instruments. Adjusting the distance in between allows the control of spray. The total ion count is affected due to the different number of ions entering the mass spectrometer. Both

the capillary voltage setting and the probe position can cause a dramatic change in ion intensity and the instrument sensitivity. This will be discussed in detail in a later chapter.

1.3 – Quadrupole Time of Flight (QTOF)

Once the gas phase analyte ions are generated in the electrospray source, they pass through a two mass analyzers (quadrupole, Q1, and TOF) and a collision cell (Q2) before reaching the detector (Figure 1.4).

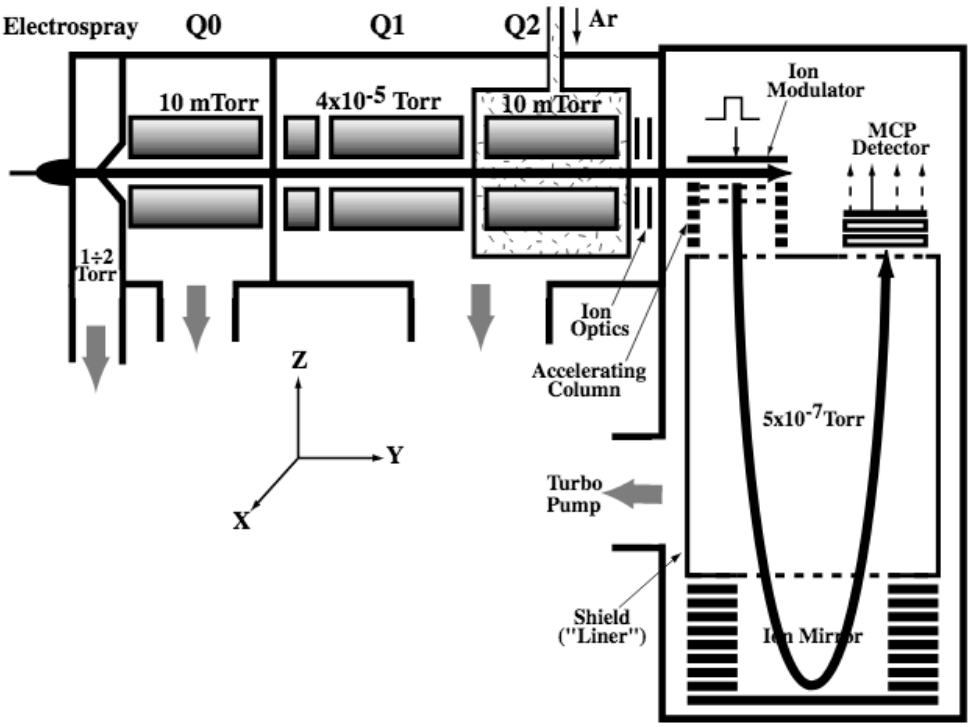

Figure 1.4 – QTOF mass analyzer. Image adapted from Chernushevich and reprint permission granted by John Wiley and Sons.[10]

Gas phase ions are generated under atmospheric pressure but enter the quadrupole under vacuum. In the instrument used in our laboratory Q0 and Q2 illustrated above are replaced by hexapoles (which cannot be used for mass analysis but are good for axial confinement of ions).

For a full scan analysis, all three quadrupoles operate under a radio frequency (rf) only mode where Q0 is used for collisional cooling and focusing of the ions entering the instrument. In a tandem mass spectrometry (MS/MS) mode, Q1 operates in a mass filter mode where a single ion of interest is selected. With an increase in the ion collision energy, Q2 operates under an argon atmosphere where collision-induced dissociation (CID) takes place. The resulting fragments, aside from the remaining parent ion, are then collisionally cooled.[11]

Tandem Mass Spectrometry, MS/MS, is a technique where a higher voltage was applied to the mass spectrometer causing fragmentations of the molecular species (Figure 1.5). Before passing through the time of flight analyzer, the gas phase ions will go through the collision gas cell with an argon gas atmosphere. The process that is involved is called the Collision Induced Dissociation (CID).

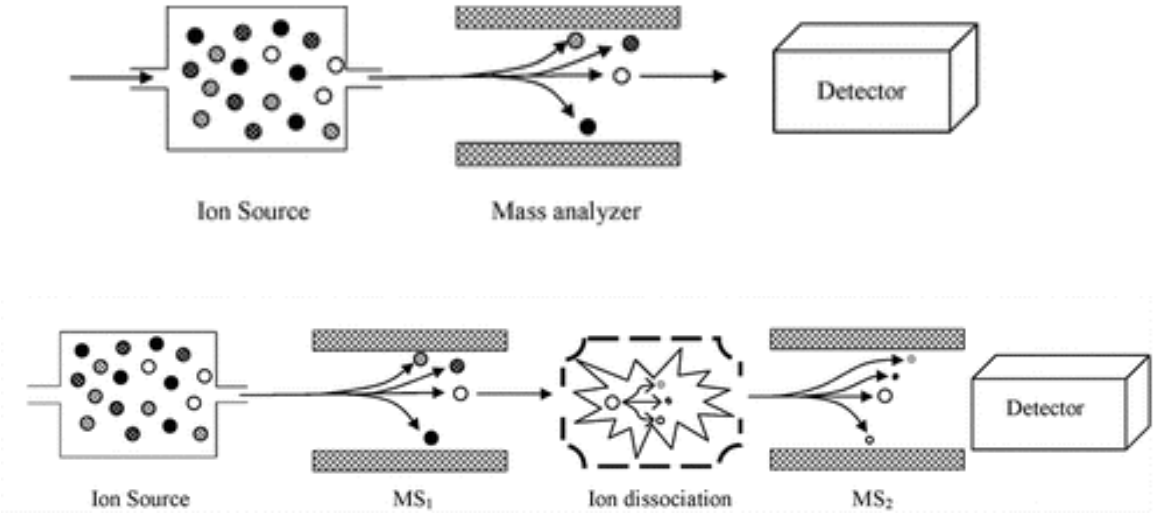

Figure 1.5 – Comparison of MS (top) and MS/MS in ESI-MS (bottom). Image adapted from El-Aneed and reprint permission granted by Taylor & Francis.[12]

As illustrated above, tandem mass spectrometry, MS/MS, allows the selection of a specific precursor ion at a specific mass number. Normally all the ions would pass through the collision cell without any hindrance. When MS/MS is performed, however, an increased collision energy and an addition of inert gas are applied to cause the fragmentation of the ions. Instead of only one peak indicating the presence of the ion species, fragmentations allow a better understanding of the structural information. It gives information regarding the composition of the ion.

One of the most useful data obtained from this technique is that it allows us to see the fragmentations, as indicated by a mass difference observed on a spectrum. Knowing the fragments and with the knowledge of the isotope pattern of the fragmentations of repeating units and molecules of interest, a better understanding regarding the structural information can be given.

After passing through the quadrupoles, ions are separated by their mass to charge ratio, *m/z*, by the time-of-flight (TOF) mass analyzer. A pulsed electric field accelerates the ions, pushing the ions in an orthogonal direction from their original trajectory. The reflectron in the analyzer then acts as an ion mirror and redirects the ions in the opposite direction in order for the ions to reach the detector. Ions with a lighter mass will arrive at the detector faster than the heavier ions based on the kinetic energy equation, $KE = \frac{1}{2}mv^2$. With constant energy and a fixed path length, the mass to charge ratios as seen from the mass spectrum are determined by the time it takes for the ions to travel the length of the flight tube until it reaches the detector.

One advantage that the reflectron offers is that the ions of the same *m/z* would arrive at the detector at the same time. Ions with the same *m/z* can have a different range of kinetic energies depending on their exact trajectory as they enter the TOF. This results in a further travel distance for the ions that have the higher kinetic energy applied upon its formation causing the ions to penetrate the reflectron field further. This ensures that the ions with the same *m/z* can arrive at the detector at the same time regardless of their initial kinetic energy. The overall effect is to enhance resolution compared to the linear time of flight considerably, and modern TOFs are capable of resolutions in excess of 30,000 FWHM (full width at half maximum).

1.4 – Detector

In this instrument, the detector used is the microchannel plate detector (MCP), and it is an array of detector with thousands of electron multiplier tubes. A mass spectrum illustrating the different intensity of species sorted by its *m/z* is generated upon the arrival of ions at the detector. This, however, could be a hindrance when multiple ions arriving at the detector are only registered as one and can be explained by the digital dead time. The digital dead time of the detector causes the over- and the under-estimation of the total ions that are present in the sample, resulting in the inaccurate quantification of data that is known as saturation.

Saturation affects the mass spectrometers at the detectors. The setting of the MCP detector voltage controls the sensitivity of the detector. In order to avoid saturation issues, the detector voltage can be de-tuned thereby avoiding the digital dead time effectively. This has to be carefully adjusted, since a detector voltage that is too low

could lead to a detection threshold, making the ions not able to register at the detector hence showing no signal on a mass spectrum.

1.5 – Background of MAO

Single-site olefin polymerization with metallocenes and methylaluminoxane (MAO) has been widely reported in the literature. Metallocenes, in combination with a traditional aluminum alkyl cocatalyst, are capable of ethane polymerization with low activity.[13] Ever since its discovery in the 1960s, methylaluminoxane (MAO) has become an important cocatalyst for metal-catalyzed olefin polymerization.[14] By simply substituting a traditional aluminum alkyl cocatalyst with MAO, the polymerization activity has been an increase by a factor of 10,000.[13] Furthermore, polymerization of ethylene, propylene, and higher α-olefins have shown a higher catalytic activity in an MAO/metallocene catalytic system.[15]

Some of the most common metallocenes used in this application are bis(cyclopentadienyl)zirconium dichloride, Cp_2ZrCl_2 or its alkylated form, bis(cyclopentadienyl)dimethyl zirconium, Cp_2ZrMe_2.[16]

1.5.1 Trimethylaluminum with Trityl Tetrakis(pentafluorophneyl)borate

Group IV metallocenes are widely used for the industrial production of polyolefins. The precatalyst dimethylzirconocene, Cp_2ZrMe_2, for example, can be activated when one of the methyl groups is abstracted from the metal centre (Scheme 1.1). The activation

chemistry can be achieved by trityl tetrakis(pentafluorophenyl)borate, $[Ph_3C]^+[B(C_6F_5)_4]^-$, and it is often performed in the presence of trialkylaluminum or alumoxane as a scavenging agent or an auxiliary activator.

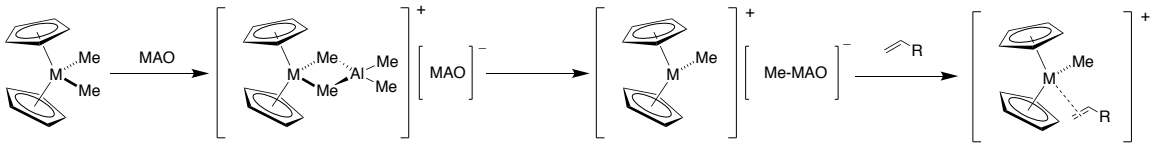

Scheme 1.1 – Olefin Polymerization with metallocene via methide abstraction.[17]

Despite being a common activator in olefin polymerization, the exact structure of MAO is difficult to characterize due to its complex set of equilibria and the lack of isolable components.[18] As different computational studies and experimental evidence have led to different proposals of the structure, one of the common observations that many have reported is the "excess" of free and unbound trimethylaluminum in the structure.[19] The amount of trimethylaluminum is crucial as it has a significant effect on the catalytic activity of MAO.[20]

With computational studies and calculations, structures of MAO can be proposed. Several proposed structures of MAO include Atwood's cyclic anion structure[21] ($Al_7O_6Me_{16}$), and Barron's and Babushkin's cage structures with bridging and terminal methyl groups (Figure 1.6).[22, 23]

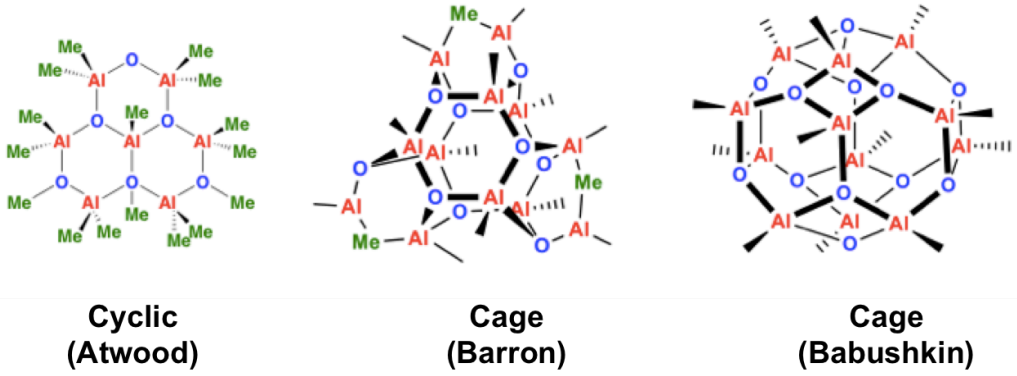

Figure 1.6 – Several proposed structures of MAO.

1.6 – ESI Studies with MAO

To gain a better insight regarding the structural composition of MAO, electrospray ionization mass spectrometry (ESI-MS) proves to be a useful technique. ESI-MS provides information regarding the composition and the molecular weight of species present in the sample. Ion-pair formation of MAO can be induced with a neutral or an anionic donor and has allowed a more thorough understanding of MAO.[24]

Upon the addition of a weakly coordinating donor, octamethyltrisiloxane, OMTS, an ion-pair formation, $[(MeAlO)_x(Me_3Al)_yMe]^-$, was observed in the negative ion mode, where the x and y each represents the different ratios between (MeAlO) and (Me_3Al) in the ion pair (Figure 1.7). MAO undergoes a $[Me_2Al]^+$ abstraction upon OMTS addition as seen in the positive ion mode, yielding a cationic complex $[Me_2Al\text{-}OMTS]^+$ (Scheme 1.2). Catalyst activation can be seen by invoking the formation of the $[Me_2Al]^+$ cation during the interaction of MAO and metallocene.[25] Understanding the reactivity of the $[Me_2Al]^+$ cation is, therefore, essential.

Scheme 1.2 – Activation of MAO upon the addition of a donor.

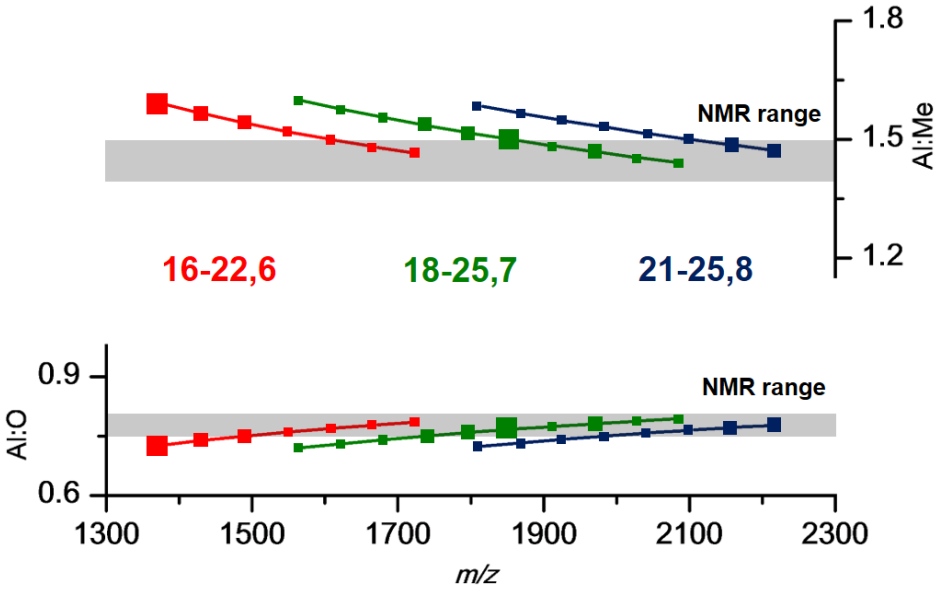

Figure 1.7 – Composition of MAO with series of $[(MeAlO)_x(Me_3Al)_yMe]^-$ ions. Reprinted with permission.[26] Copyright 2017 American Chemical Society.

Experimental results reported from Kaminsky showed the linear dependency of reaction rate on the ratio of zirconium to aluminum. A high ratio between MAO and metallocene is typically required for an olefin polymerization reaction, as the optimal ratio of Al/Zr between the MAO and metallocene in a reaction lies up to 5000:1 with certain systems requiring up to 10,000.[27] The cost of the excess MAO is a disadvantage in comparison to Ziegler-Natta catalysts.[28]

Upon the addition of OMTS to MAO, a donor-stabilized complex $[Me_2Al\text{-}OMTS]^+$ is observed. Effective methyl abstraction from the donor-stabilized complex reported from literature has demonstrated the outstanding ability for catalyst activation.[25] Therefore, the

alternative approach is to focus specifically on the reactive site on MAO. As previously mentioned, the Lewis acidic moiety of the dimethylaluminum cation, $[Me_2Al]^+$, plays an important role in the catalytic activity. Focusing on the reactive part of MAO gives direct studies and more insight in terms of how the reactions proceed with the presence of catalysts and just the reactive part of the activator. To investigate the reactivity of $[Me_2Al]^+$, it is crucial to stabilize the cation with a weakly coordinated donor. Using trimethylaluminum instead of MAO would not require a ratio as high as the MAO/metallocene complex. With a lower Al/Zr ratio and with the substitution of trimethylaluminum in contrast to MAO, a more in-depth structural and reactivity study can be done.

Alkyl abstraction of trialkylaluminums was observed upon the addition of a boron activator $B(C_6F_5)_3$.[29] Donor-stabilized dimethylaluminum cationic complexes are known to activate metallocene complexes and proceed to olefin polymerization.[30] With the aim of lowering the Al/Zr ratio, the original objective of the experiment is to discover the optimal ratio and weakly coordinated donors that yields the optimal outcome of an olefin polymerization reaction with metallocenes (Scheme 1.3).

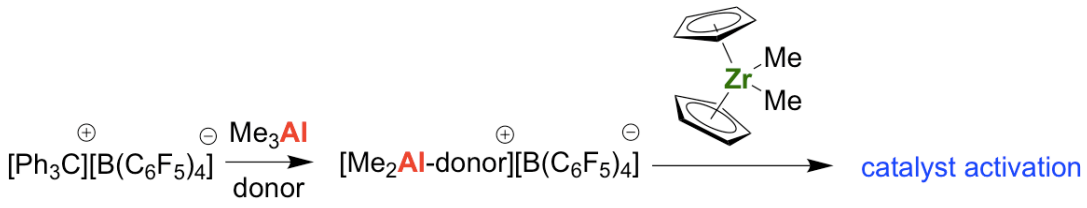

Scheme 1.3 – Catalyst Activation with donor-stabilized dimethylaluminum cation.

Group 13 activators that contain boron and aluminum have seen wide applications in olefin polymerization. Boron activators, $B(C_6F_5)_3$, $[PhNMe_2H]^+[B(C_6F_5)_4]^-$, and $[Ph_3C]+[B(C_6F_5)_4]^-$ have been widely used in applications such as single-site olefin polymerization.[31, 32] They have been used a hydride or methide abstracting agent due to their Lewis acidity[33] and its role as a key component in a homogeneous single-site olefin polymerization system has been reported.[34] Trimethylaluminum, Me_3Al, has shown to be a potent activator in olefin polymerization.[14] The hypothesis is that the boron activator serves as the methyl abstracting agent of the trimethylaluminum. The addition of an electron donor stabilizes the reactive dimethylaluminum cation, $[Me_2Al]^+$, forming a stabilized $[Me_2Al\text{-donor}]^+$ complex, which then facilitates the activation of a metallocene complex. The reaction eventually proceeds to olefin polymerization by abstracting a methyl group from the metallocene.

The methyl abstracting nature of the boron activator, also the coordinating anion, $[B(C_6F_5)_4]^-$ can be seen in the facile alkyl exchange. Structures such as $Al(C_6F_5)_4$ and BMe_3 serve as evidence.[35] The degradation of $[B(C_6F_5)_4]^-$ upon its reaction with trimethylaluminum can be written as $AlMe_{3-x}(C_6F_5)_x$ where different ratios of Al/B yields different ratios of products (Scheme 1.4).[29]

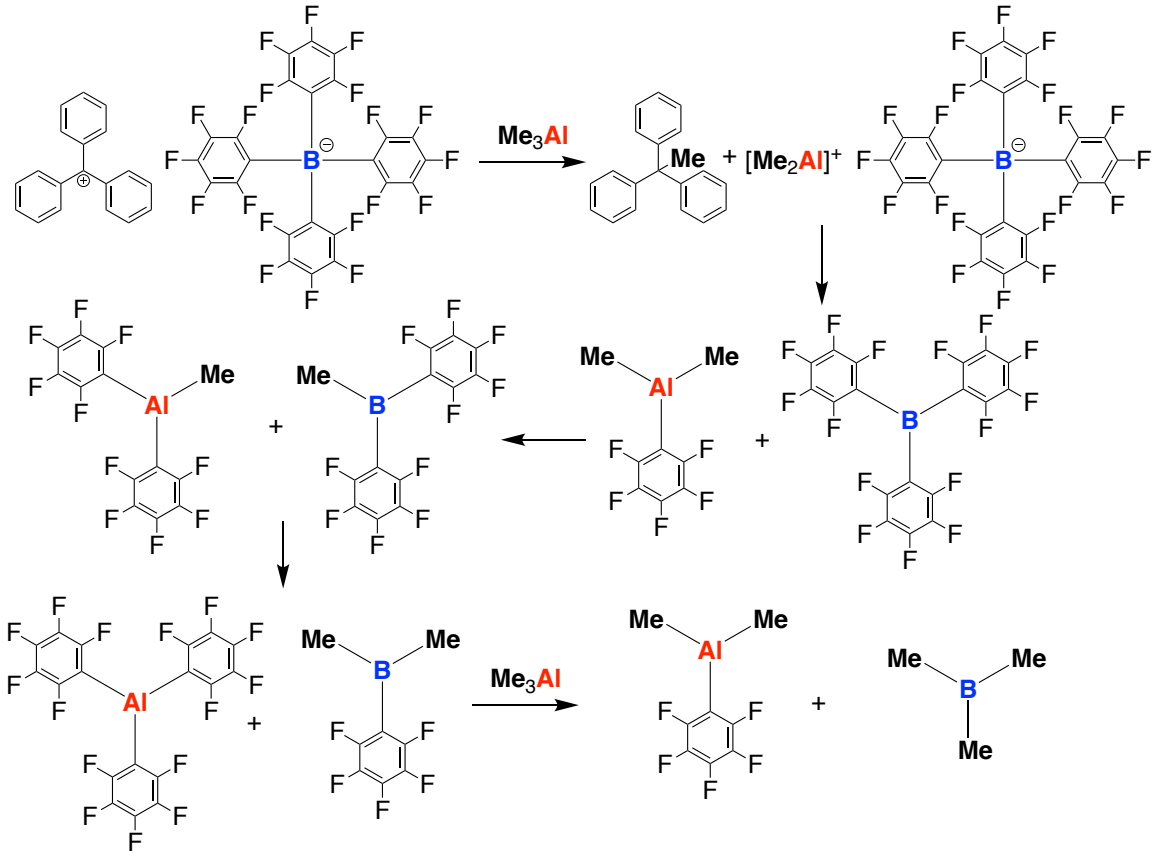

Scheme 1.4 – Reaction Scheme of trimethylaluminum addition to trityl reported from Bochmann.[29]

Upon addition of trimethylaluminum to trityl tetrakis(pentafluorophenyl)borate, $[Ph_3C]^+[B(C_6F_5)_4]^-$, demethylation of trimethylaluminum and a methylated trityl carbocation onto the carbocation centre, confirmed with ^{19}F NMR, has been previously reported in the literature (Scheme 1.5). Due to the neutrality of the methylated product, it cannot be observed with ESI-MS.

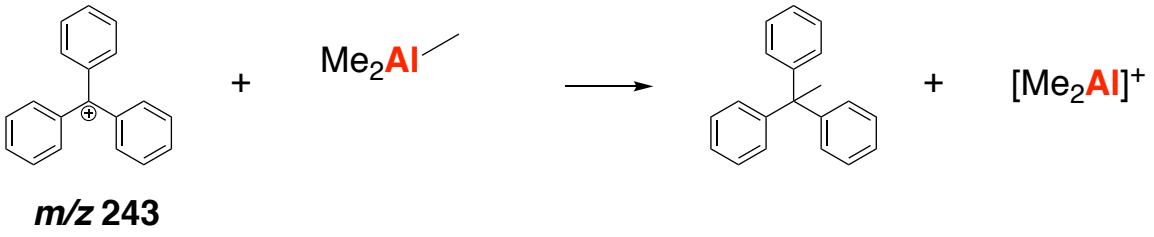

Scheme 1.5 – Reaction scheme reported with the synthetic route of the methyl addition to the carboncation centre.[29]

Structural changes of the phenyl ring of the trityl carbocation have however never been reported. In a newly discovered reactivity, the methyl abstraction from trimethylaluminum that results in the hydride abstraction and the methyl addition of a phenyl ring on the carbocation is a new reaction that will be discussed in a later chapter. This was an interesting discovery that came up during the investigation of the activation chemistry. Upon the addition of trimethylaluminum, an unknown +14 Da species was observed via on a positive ion mode mass spectrum. Due to the mass to charge ratio, the $-CH_2$ addition on the phenyl ring of the trityl cation instead of the carbocation centre alongside the demethylation of the trimethylaluminum was the hypothesis.

Bochmann has previously conducted experiments and investigations regarding the addition of trialkylaluminums to trityl tetrakis(pentafluorophenyl)borate. With various trityl to trialkylaluminum ratios, different species were observed with ^{1}H and ^{19}F NMR NMR. Adjusting the Al/B ratios from the two reagents varied Aryl/alkyl exchange reactions (Figure 1.4).

No experiments regarding the addition of trimethylaluminum to trityl carbocation with ESI-MS have been reported. The demethylation of trimethylaluminum and the $-CH_2$

addition onto the phenyl ring of trityl carbocation has also not been previously reported in the literature. Experimental results comparing different solvents and different molar equivalences of trimethylaluminum addition are reported. By applying the optimal settings of the instrumental parameters that effectively avoided the saturation issue, spectra under saturated and non-saturated conditions are also compared with a direct study of the trityl carbocation chemistry.

Chapter 2 – Avoiding Saturation Effects in Concentrated Samples

2.1 – Background

Mass spectrometry is well known for its sensitivity. Improvements in instrumentation and methodologies have in recent years been developed with the aim of a lower detection limit, and astonishing feats of characterization have been achieved as a result.[36] Having a very sensitive technique while monitoring highly reactive compounds can however be a disadvantage. Despite the ability to measure samples at low concentrations, highly reactive compounds will react rapidly and deleteriously with traces of moisture and oxygen, which are hard to remove below 5 ppm in the solvent. Preparing the reactive compounds at a higher concentration can solve this issue; nonetheless, samples with a higher concentration can lead to another issue: saturation. Saturation is a very common issue, as it can be observed in various reaction monitoring analytical measurements. With different detection limits and dynamic range, it is important to find the optimal concentration range with a linear relationship between intensity and sample concentration.

2.2 – Saturation in mass spectrometry

For a reaction with a 100% conversion rate, the amount of reactant used should correspond to the amount of product produced as seen on the abundance vs. time traces. When there is a bigger change in the product trace compared to the reactant trace, it can

be said that the reaction is saturated and the data does not reflect the actual changes in concentration.

The figure below (Figure 2.1) illustrates the reactant trace in red and the product trace in blue. Upon addition of triisobutylaluminum, *i*Bu_3Al, to trityl carbocation, $[Ph_3C]^+$, the over-representation of the product trace and the under-representation of the reactant trace is a clear sign that saturation was affecting the data.

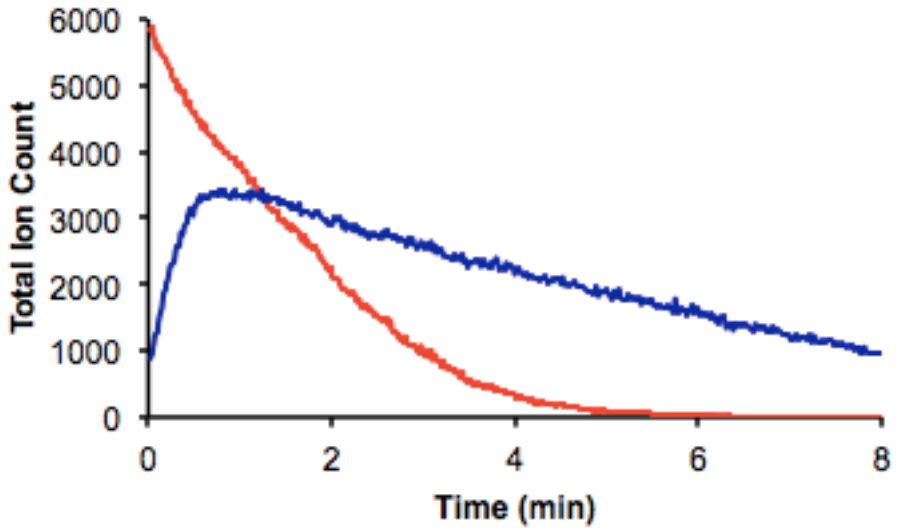

Figure 2.1 – An example of a saturated condition upon addition of *i*Bu_3Al to $[Ph_3C]^+$ showing a bigger change in the product trace (blue) than the reactant trace (red).

ESI-MS offers a very sensitive measurement of the quantity of ions present in the sample. Accurate quantification with ESI-MS has proved to be a much bigger challenge due to the ultra-sensitive nature of the instrument. The challenges of the quantitative characterization of supramolecular complexes have been previously reported.[37] Studies regarding the challenges with quantification of the thermodynamic equilibrium constants and the concentration of metal complexes present in the spectra have been briefly described.[38] In this chapter, the challenges of the accurate quantification of analyte

concentration will be addressed. Moreover, the saturation issue will be investigated, as it is the primary cause of poor quantification. Overcoming the issue will allow accurate and quantitative reaction monitoring, which is the primary goal of this project.

In general, an ideal spectroscopic method that allows for the determination of the sample concentration would have a high dynamic range and a linear calibration curve extending over a good number of orders of magnitude. Depending on the analyte, a linear calibration curve could be established over a different range of concentrations with a combination of different parameters for the instrument. Varying the solvents and the coordinating cation or anion of the analytes[39], it could have a significant effect on the outcome due to the spray quality and the interaction between the ions.[40] Losing the linearity of a calibration curve indicates the measurements can no longer reflect the true concentration in the sample. Similar experiments have been conducted and reported where the loss of linearity can be seen when the sample investigated exceeds the maximum concentration.[41]

Mass spectrometry is not the only analytical method that suffers from signal saturation. Below is a comparison between a commonly used reaction monitoring spectroscopic method and ESI-MS. For infrared spectroscopy (IR), a "plateau" can be seen when the concentration of the analyte increases. While the signal intensity can no longer reflect its “true” concentration or when the calibration curve loses linearity as the concentration increases, a saturated phenomenon is seen (Figure 2.2).

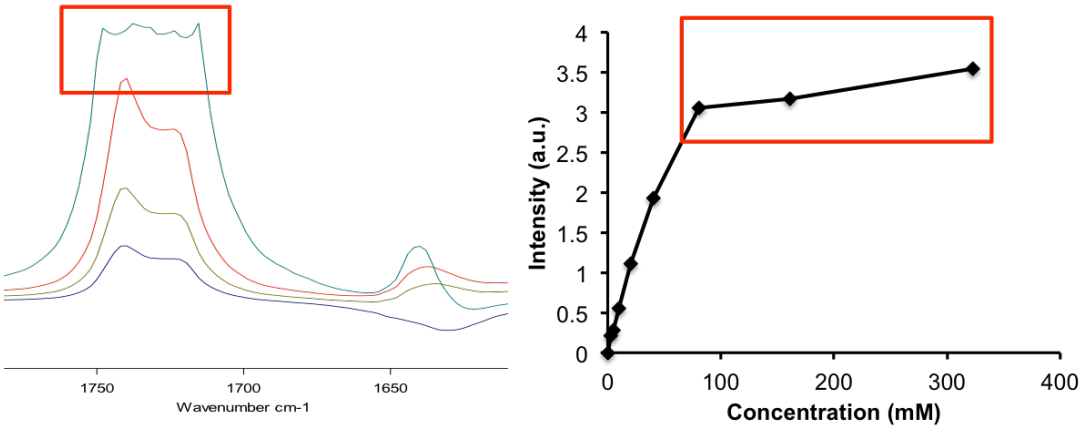

Figure 2.2 – IR spectra of dimethyl itaconate. (Left) Saturation indicated by distorted peak shape. (Right) Loss of linearity indicated by the concentration range. Experiment conducted by Miller.

Different spectroscopic methods have different ranges of concentration where the saturation is observed. As illustrated above, the concentration range where saturated condition can be seen on an IR spectrum at concentrations higher than 100 mmol/L (Figure 2.2). For ESI-MS however, due to the higher sensitivity, the maximum concentration before the calibration curve loses its linearity is significantly lower. For a concentration above 60 µmol/L (Figure 2.3), the calibration curve loses linearity. This indicates the mass spectrum above this concentration is no longer reliable for quantitative studies, as the ion intensity can no longer accurately reflect the true concentration of the analyte.

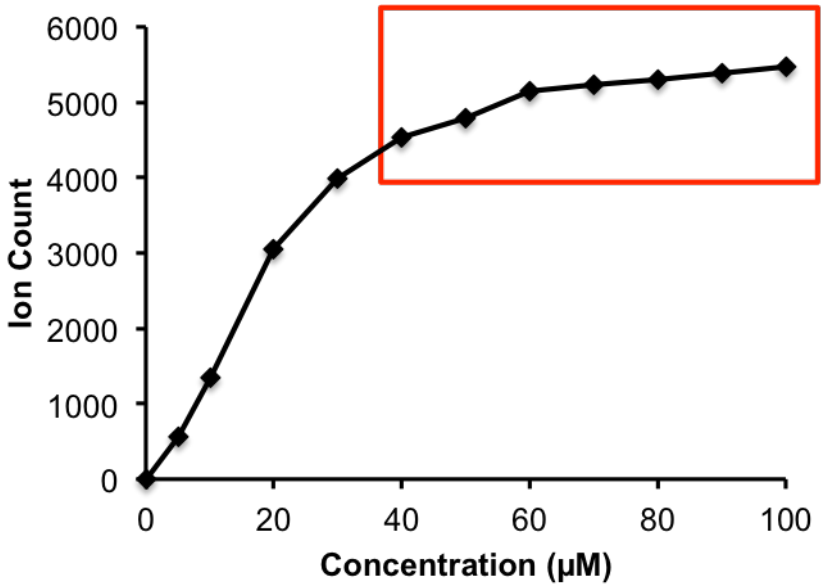

Figure 2.3 – ESI-MS saturation and the concentration range for trityl cation.

There is other evidence that indicates saturation on a mass spectrum. When monitoring a reaction, the traces of ion peaks that indicate the abundance of different species can give a clear idea regarding saturation. Having an irregular isotope pattern, a distorted baseline for ion peak and an over-representation and under-representation of ion peaks can serve as evidence of signal saturation.

Saturation issues were first recognized when the abundance of the product was over-represented, and the abundance of reactant was under-represented on the spectrum. To solve the issue, it was essential to adjust the sensitivity of the instrument. Working in reverse, we are attempting to reduce the sensitivity of the instrument by de-tuning various parameters. When the sensitivity of the instrument proves not to be beneficial to the experimental results, reducing its sensitivity is a key route to acquire more accurate data.

By simply tuning the various parameters of the instrument, a notable difference and a better and more accurate measurement can be seen on product and reactant traces.

Experimental results can be significantly affected by different settings of the instrument. Desolvation gas temperatures, probe positions, and flow rate[3] can significantly affect the outcome of the results. The effects of the above-mentioned instrumental parameters have been previously reported in the literature.[42] To allow a better understanding of the instrumental settings and optimization, this chapter will investigate the effects of adjusting different parameters and compare the outcomes regarding the sensitivity.

2.2.1 Isotope pattern

Signal saturation disproportionately affects the most dominant peak in the spectrum (Figure 2.4). The isotope pattern of the sample can be calculated.[43] It contains peaks of different intensity depending on the composition of the species according to the abundance of the element. However, they are affected to a different degree, as smaller peaks would appear larger than it should be and the largest peak would then appear less intense than calculated. Experimental results can be compared to the calculated results and the saturation issue can be easily identified.

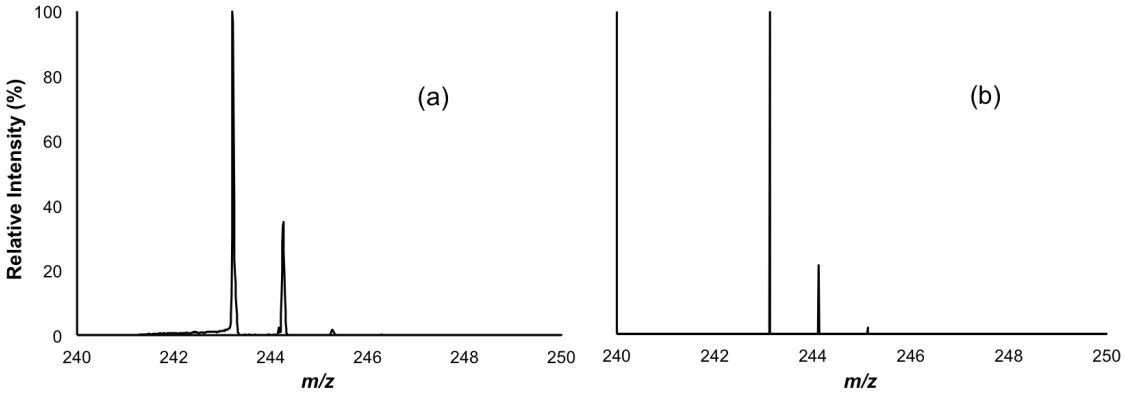

Figure 2.4 – ESI-MS isotope pattern of $[Ph_3C]^+$. (Right) Saturated isotope pattern. (Left) Non-saturated isotope pattern calculated by ChemCalc.

Comparing the calculated and saturated isotope pattern of trityl carbocation (*m/z* 243 Da), the M+1 peak is twice the abundance than the calculated spectrum. This inconsistency points to the fact that signal saturation causes the inaccuracy.

2.2.2 Baseline Distortion

For the time of flight (TOF) mass analyzers the distortion at the base of the peak is an indication of saturation. A distinct ramp before the peak and a pronounced tailing afterward can be seen (Figure 2.5).

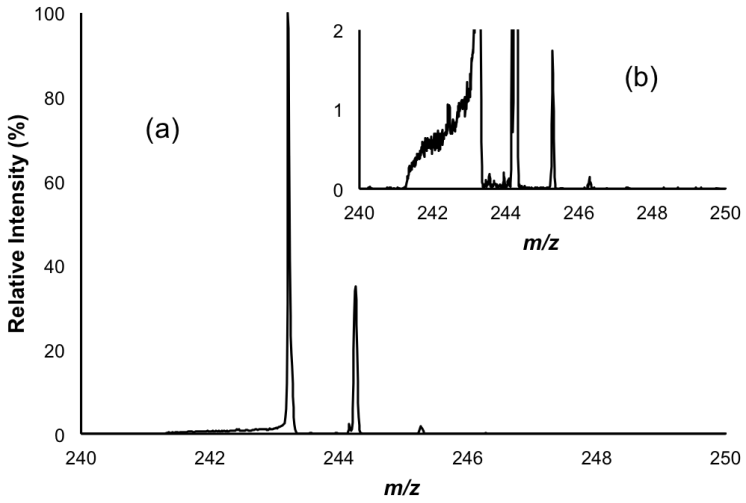

Figure 2.5 – A non-saturated baseline peak of $[Ph_3C]^+$ with a zoomed-in baseline distortion indicating saturation.

2.2.3 Reaction traces of Isotope pattern M, M+1, and M+2

Carbon has two naturally occurring isotopes (^{13}C and ^{14}C) that can be easily observed with hydrocarbon species in ESI-MS.[44] Ion saturation regarding the ion abundance from the isotope pattern can be compared and studied.[45] Another indication of a saturated mass spectrum can be identified by comparing all the reaction traces from M, representing the *m/z* of the species, and its isotope pattern, M+1, and M+2.

A notable difference can be seen while comparing the traces (Figure 2.6). A quick test can identify whether the conditions are saturated. Under normal condition, normalized traces should overlay for the traces. For hydrocarbon species, signal saturation can be observed when the traces of M do not resemble the traces in M+1 and M+2.

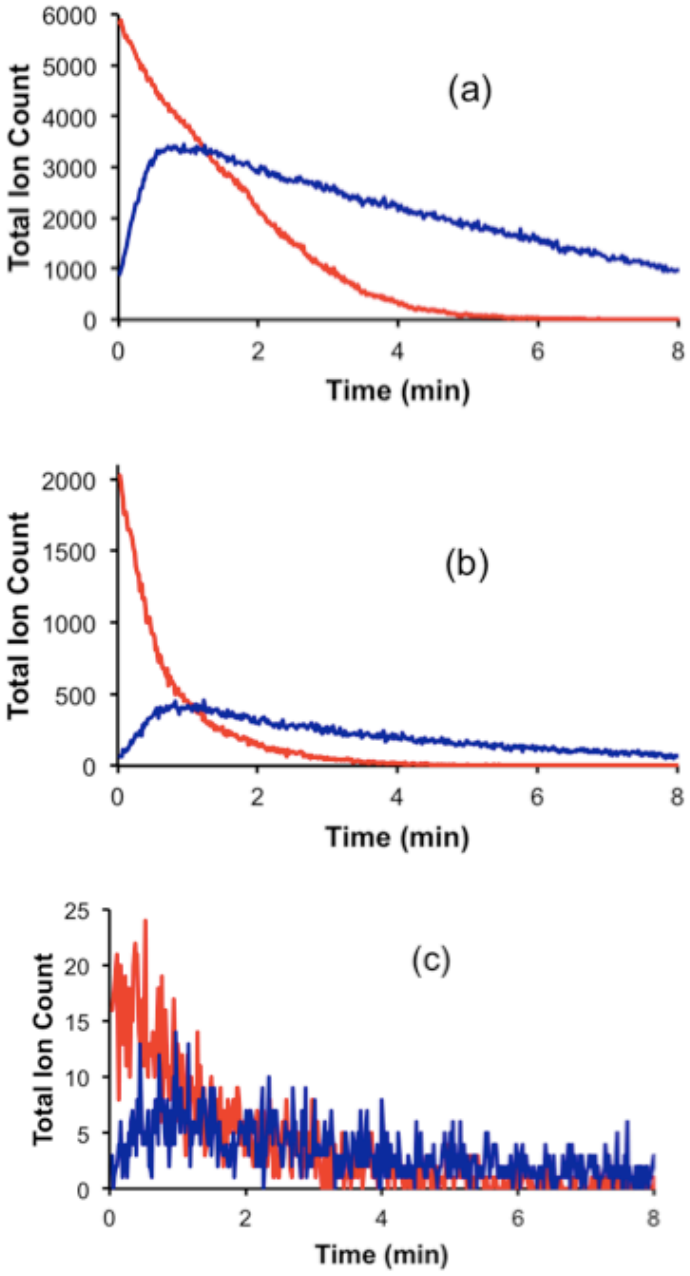

Figure 2.6 – Comparison of traces of ion peak of $[Ph_3C]^+$ and $[Ph_2C\text{-}C_6H_4iBu]$ at (a) M (*m/z* 243 and *m/z* 299) (b) M+1 (*m/z* 244 and *m/z* 300) (c) M+2 (*m/z* 245 and *m/z* 301).

2.2.4 Quadrupole Resolution

Aside from the distortion of the peak shape indicated by the baseline of the isotope pattern, another distorted peak shape can suggest the saturation issue (Figure 2.7). A truncated surface obtained from a mass spectrum is another indication of a signal saturation.

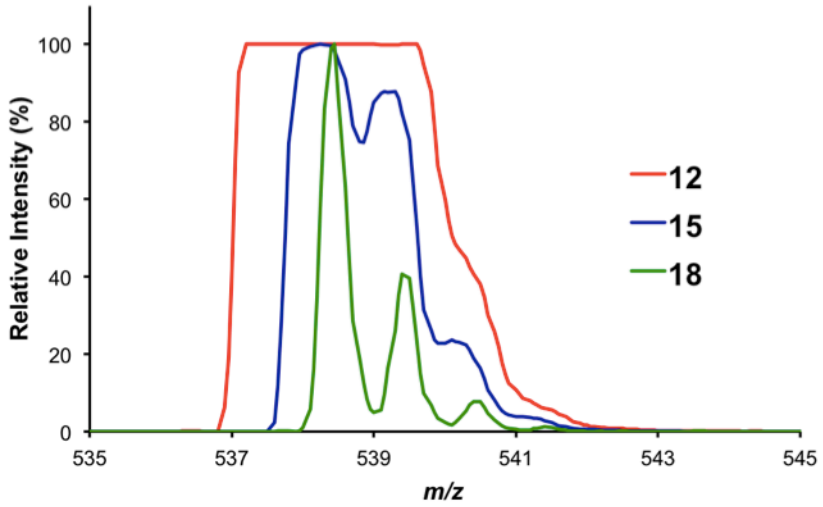

Figure 2.7 – ESI-MS(+) saturation indicated by quadrupole resolution. (Red) Saturation indicated by a truncated surface. (Blue and green) Non-saturated peak.

2.3 – Overcoming the limitations

The rule-of-thumb while encountering saturation prior to this project would simply be reducing the concentrations further to avoid the issue. This is not effective when dealing with highly reactive compounds due to the decomposition of the sample. Due to the highly reactive nature of trityl carbocation, $[Ph_3C]^+$, traces of moisture and oxygen with just a few ppm in concentration can decompose the sample. Because of that, a minimum

concentration that avoids the sample decomposition is required.[46] The trade-off and the disadvantages of running the mass spectrometer with both high and low sample concentrations are tabulated. Bearing the difficulties in mind, we can see that by simply diluting the sample concentration proves to be insufficient and ineffective. In order to overcome such limitations, the effects of de-tuning and adjusting various instrumental parameters were performed (Table 2.1). Lowering the sensitivity of the instrument, however, also comes with a number of disadvantages that will be discussed later on in this chapter.

High Concentrations	**Low Concentrations**
Advantages	
- Faster reaction rate	- A better linear response that corresponds to the actual concentration
Disadvantages	
- Ion suppression - Data saturation	- Slower reaction rate - Analyte decomposition caused by traces of impurities

Table 2.1 – Advantages and disadvantages of high and low sample concentrations.

The importance of finding the sweet spot in between having a high enough concentration and setting of parameters to avoid saturation is important. In order to keep the optimal reaction rate and achieve a calibration curve that reflects the true concentration of the

sample, the combination of the optimal settings need to come together. With the optimal concentration and the optimal setup of the parameters, an accurate measurement of the data can be assured, and the correct quantification of species present in the reaction can, therefore, be reported.

Mass spectrometer can be divided into three main operations, ionization, mass analysis, and detection. Parameters that correspond to different operations of the instrument can be adjusted individually to yield optimal results and sensitivity.

For example, the probe position (the distance between the probe and the cone of the instrument) can be adjusted to favour formation of gas phase ions after solvent evaporation allowing the analyte ions to be better quantified was seen.[47,8] By varying the capillary voltage and the gas flow, the ionization efficiency regarding the droplet evaporation and electrochemistry can be affected.[48] A more accurate mass spectrum can be acquired with the optimal settings of the two parameters.[49] The importance of a threshold concentration that allows the detection of the analyte and avoids sample decomposition has also been an emphasis for mass spectrometric studies and has been helpful when selecting an optimal concentration range for reactive compounds.[50] Fixing the saturation issue with computational method proves to be effective, as reported literature utilizes an algorithmic correction whereby an unsaturated peak in an isotope pattern is used to work backward that allows a better and more accurate estimation of the abundance of the peak.[51]

2.3.1 Parameters Adjusted

On top of diluting the concentrations of the sample, de-tuning various parameters when acquiring the spectrum can optimize the ion count. However, optimization can cause a misrepresentation of different species. In this study, trityl carbocation, $[Ph_3C]^+$, was examined. It is a permanently positively charged cation used for methide or hydride abstraction[52], which is paired with a negatively charged weakly coordinated anion, $[B(C_6F_5)_4]^-$. It is an easily detectable trace for ESI-MS, however, due to its highly reactive nature, an optimal range of concentrations was selected in order to give a reasonable detection and high enough to avoid the decomposition of the sample that could potentially occur.

Capillary voltage, probe position, cone gas flow rate, and MCP detector voltage are the four parameters that are selected to optimize the representation of each species while ensuring that the ion count reflects the correct quantity of the ion. Probe position can have a significant impact on ion count. The goal of this experiment is to combine the most optimal concentration, capillary voltage, MCP detector voltage, flow rate, and probe position to ensure an accurate representation of the ion showed in the spectrum.

Detuning the instrument is one of the top priorities in this study, though it also comes with its pros and cons. By detuning the instrument, a more linear response can be obtained, corresponding to the accurate quantification of the molecular species. However, by detuning the instrument, a threshold appears, proving that parameters that are detuned must remain at a certain number or higher. Therefore, to find a sweet spot in between where the quantification is accurate and the response is linear to the increase of sample concentration is the most important goal in this thesis.

2.3.2 Capillary Voltage

The capillary voltage produces a Taylor cone and spray of fine charged droplets. By de-tuning the capillary voltage, the number of ions generated can be decreased, though not below the point at which a stable spray is formed.

2.3.3 MCP Detector Voltage

A microchannel plate (MCP) is a detector that consists of a closely packed array of electron multipliers that can detect ions arriving over a wide area. A time-to-digital converter (TDC) is usually coupled with the detector and sets up timing increments separated by intervals of less than a nanosecond.[53] Ions registered at the detector are then processed, and a mass spectrum is generated.

At a given time window, the detector can only register one event. A phenomenon where the arrival of multiple ions is only registered as one ion can be described by the digital dead time.

The MCP detector voltage has a significant effect on the sensitivity of the instrument. With a decrease in the detector voltage, the sensitivity is, therefore, turned down. This, however, leads to another discussion in terms of an optimal setting. If the voltage has been too insensitive, a "threshold" is observed; hence a minimum value of the MCP detector is required to avoid the issue.

2.3.4 Probe Position

Some mass spectrometers allow the adjustment of the probe position on the x- and y-axes. It is the distance with respect to the orifice of the instrument where the gas phase ions are introduced. By simply adjusting the distance a few millimeters, a dramatic change can be observed as the signal intensity could increase or decrease drastically, with smaller, more mobile ions losing less intensity with respect to their bulkier counterparts at greater distances.

When the x and y-axes are adjusted, the spray can be controlled, and the sensitivity of the instrument can be significantly tuned and detuned. As the grid suggested, five probe positions were investigated (Figure 2.8).

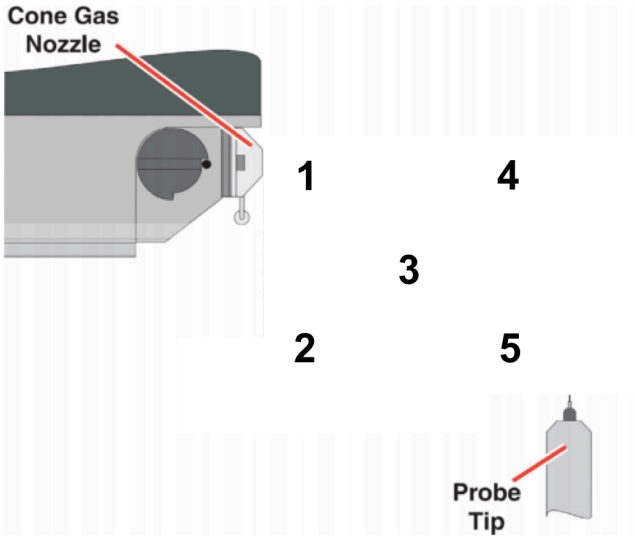

Figure 2.8 – Probe positions (capillary to cone distance) of the instrument investigated. Position 1 (x = 1 mm, y = 3 mm). Position 2 (x = 1 mm, y = 6 mm). Position 3 (x = 5 mm, y = 4.5 mm). Position 4 (x = 10 mm, y = 3 mm). Position 5 (x = 10 mm, y = 6 mm).

2.3.5 Cone gas

The instrument has two gas sources, the desolvation gas, and the cone gas. Optimizing the desorption and ionization process to enhance spectral quality has been reported.[54] By adjusting the desolvation gas flow of the instrument, an enhancement in sensitivity and optimization of the abundance of characteristic fragmentations in biochemical studies have been can be seen.[55]

The desolvation gas is a coaxial flow heated nitrogen gas at a high flow rate emerging from around the capillary, and the cone gas is the flow that emerges from the cone mounted at the orifice of the instrument. Increasing the cone gas flow increases desolvation but comes at the cost of the difficulty for the ions to make it into the source of the instrument (ions are "blown away" from the entrance to the mass spectrometer). Investigating the effect of cone gas allows a better understanding to tackle the saturation issue, as it also has an effect on the ionization efficiency affecting the droplet evaporation.[42]

2.4 – Experimental

Trityl carbocation (1.00 mg, 1.08×10^{-6} mol) was weighed out, and fluorobenzene (10.0 mL) was added to make a solution of 1.00×10^{-4} M. A one-millilitre sample is prepared for trityl at twelve different concentrations by adding different volumes of stock trityl solution and fluorobenzene (Table 2.2).

Sample was then injected via direct sample infusion with a 1 mL syringe and a syringe pump through PTFE tubing. The flow rate was set at 20 μL/min. Mass spectrum was

obtained for one minute, where an average the total ion count at the peak *m/z* +243 Da was taken.

In the experimental setup, probe position 1 (Figure 2.10), 2 (Figure 2.11), 3 (Figure 2.9), 4, and 5 (Figure 2.12) were investigated one at a time. Keeping the flow rate constant, capillary voltages and MCP detector voltages were thoroughly investigated. An increment of 250 V from 1750 V to 3000 V was selected for capillary voltage. For MCP detector voltage, an increment of 200 V between 2100 V and 2700 V were investigated. Once the data for all the combinations of capillary voltages and MCP detector voltages of a fixed probe position were acquired, experiments were continued with the investigation of another probe position.

Concentration ($\times 10^{-5}$ mol/L)	Volume of prepared trityl solution (1×10^{-4} mol/L)	Volume of fluorobenzene added (mL)
0.5	0.05	0.95
1	0.1	0.9
2	0.2	0.8
3	0.3	0.7
4	0.4	0.6
5	0.5	0.5
6	0.6	0.4
7	0.7	0.3
8	0.8	0.2
9	0.9	0.1
10	1	0

Table 2.2 – Sample concentrations of $[Ph_3C]^+$ prepared.

2.5 – Results

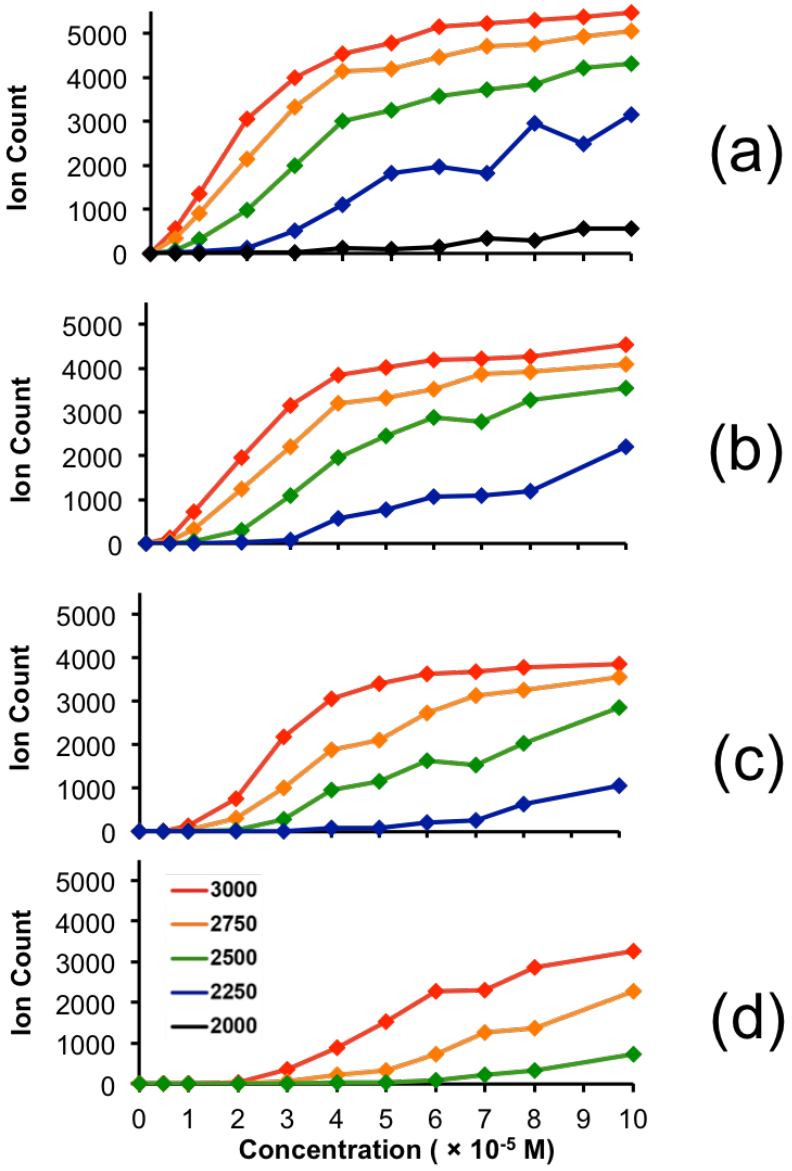

Figure 2.9 – Calibration curves at probe position 3. Each spectrum represents a different MCP detector voltage. (a) 2700 V (b) 2500 V (c) 2300 V (d) 2100 V. Legends indicate different capillary voltages. Cone gas held at 50 L/hour and probe position held at position 2.

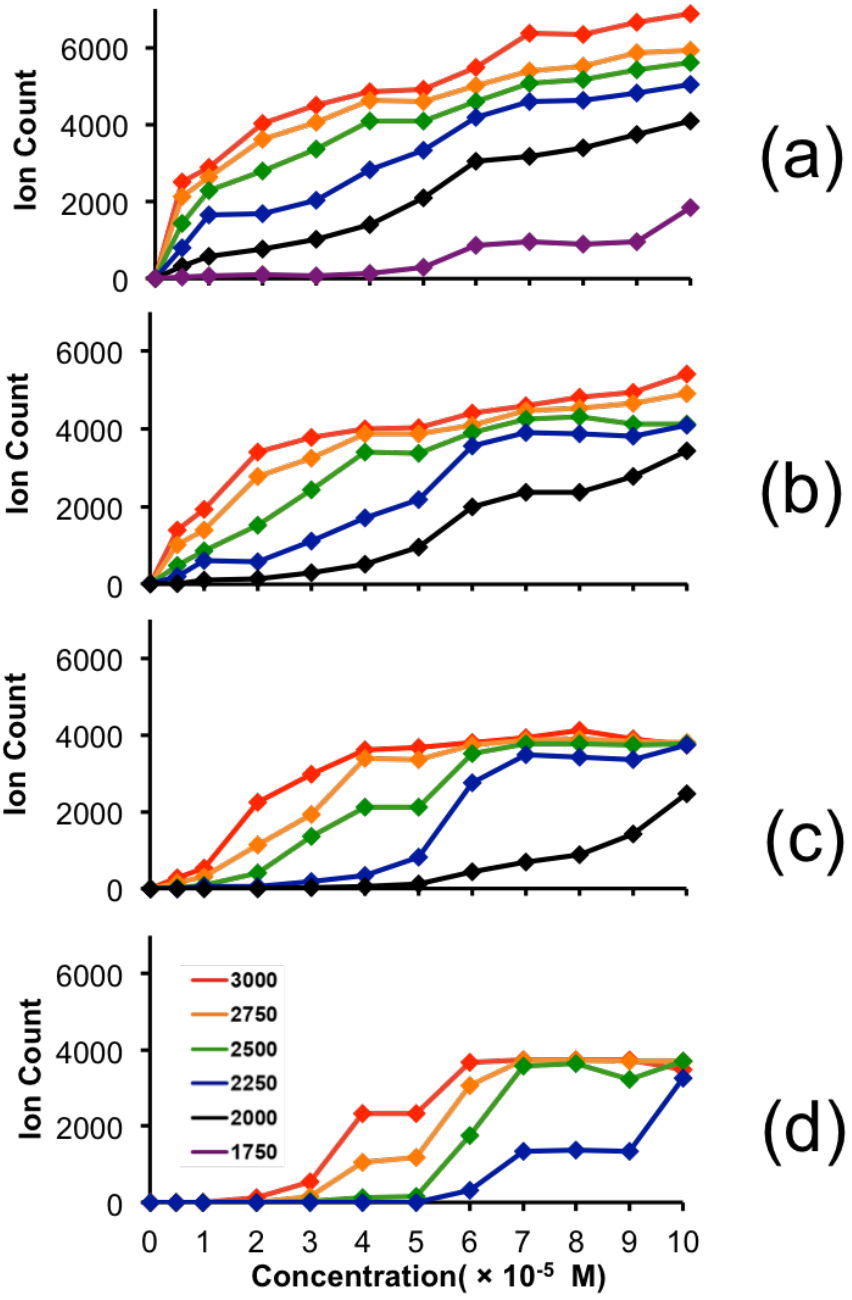

Figure 2.10 – Calibration curves at probe position 1. Each spectrum represents a different MCP detector voltage. (a) 2700 V (b) 2500 V (c) 2300 V (d) 2100 V. Legends indicate different capillary voltages. Cone gas held at 50 L/hour and probe position held at position 2.

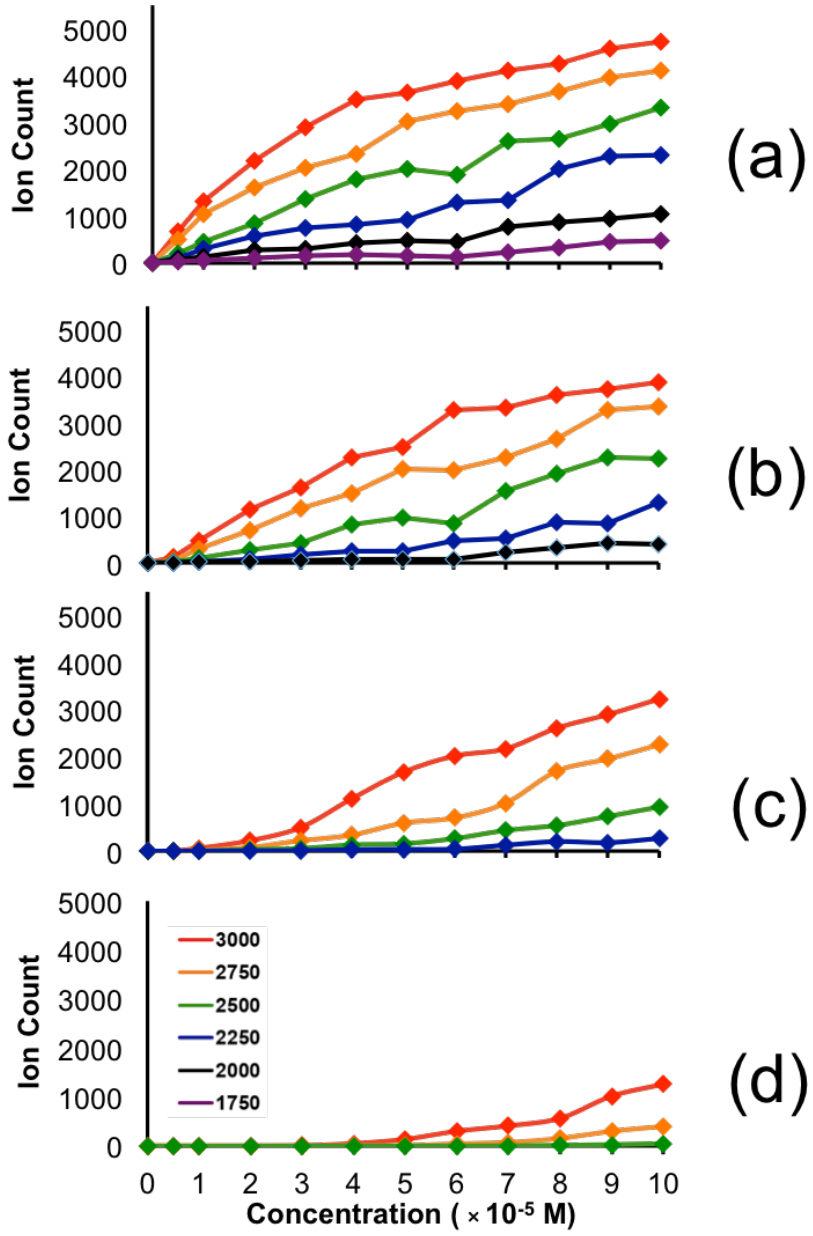

Figure 2.11 – Calibration curves at probe position 2. Each spectrum represents a different MCP detector voltage. (a) 2700 V (b) 2500 V (c) 2300 V (d) 2100 V. Legends indicate different capillary voltages. Cone gas held at 50 L/hour and probe position held at position 2.

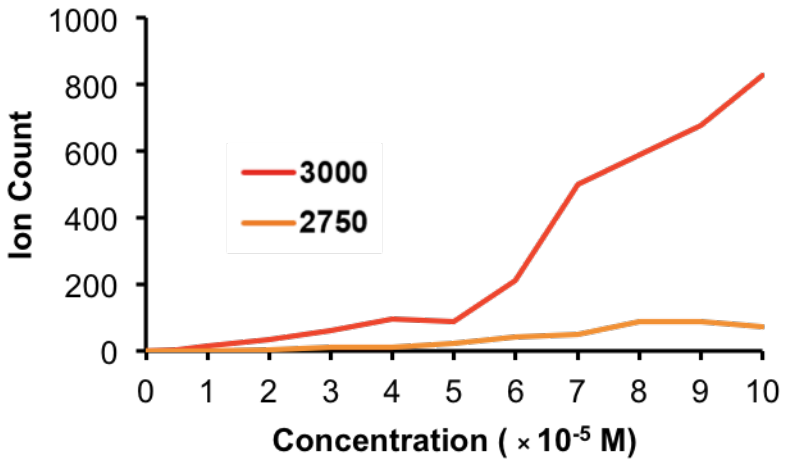

Figure 2.12 – Calibration curves at probe position 5 with MCP detector voltage at 2700 V. Legends indicate the capillary voltages. Cone gas held at 50 L/hour and probe position held at position 2.

Adjusting the previously mentioned parameters in the instrument, capillary voltage, probe position, cone voltage, and detector voltage should ideally generate a linear calibration curve where an increase of concentration should be followed by an increase of ion intensity as reflected on the mass spectrum. The technique to discover the perfect solution proved to be challenging, as an optimal combination of all the parameter settings needs to take place to generate such a calibration curve. For that reason, it is best to hold three of the parameters mentioned above constant while adjusting the MCP detector voltage (Figure 2.13), the capillary voltage (Figure 2.14), the probe position (Figure 2.15), and the cone gas flow (Figure 2.16). This allows the direct observation of the resulting spectrum that highlights the effect of a specific parameter.

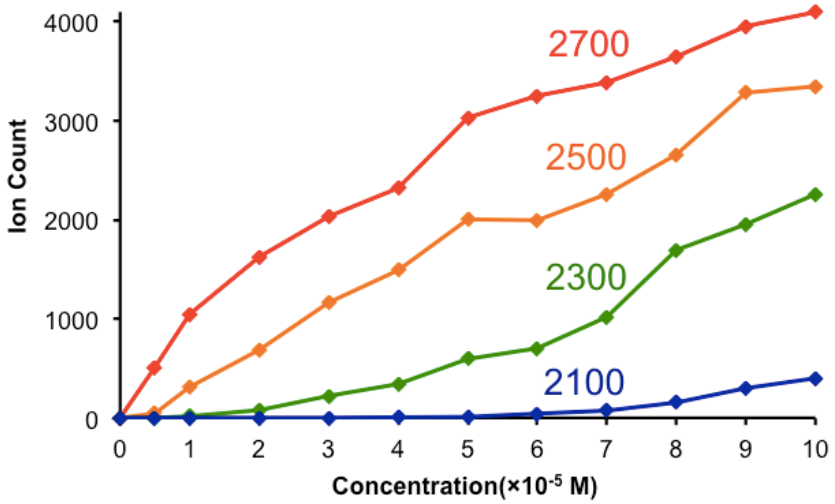

Figure 2.13 – A calibration curve of $[Ph_3C]^+$ with a fixed cone gas flow (50 L/hour), probe position (2), and capillary voltage (2750 V). Each colour represents a different MCP voltage setting.

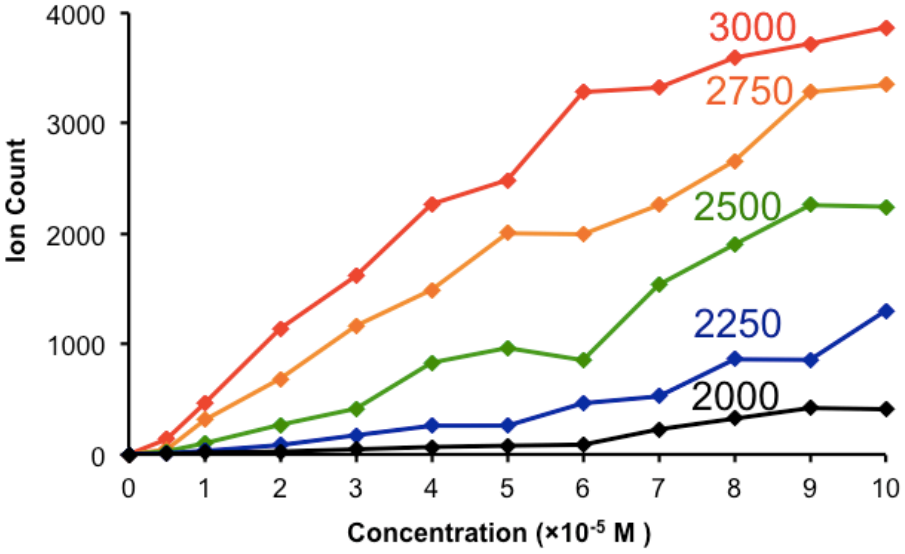

Figure 2.14 – A calibration curve of $[Ph_3C]^+$ with a fixed cone gas flow (50 L/hour), probe position (2), and MCP voltage (2500 V). Each colour represents a different capillary voltage setting.

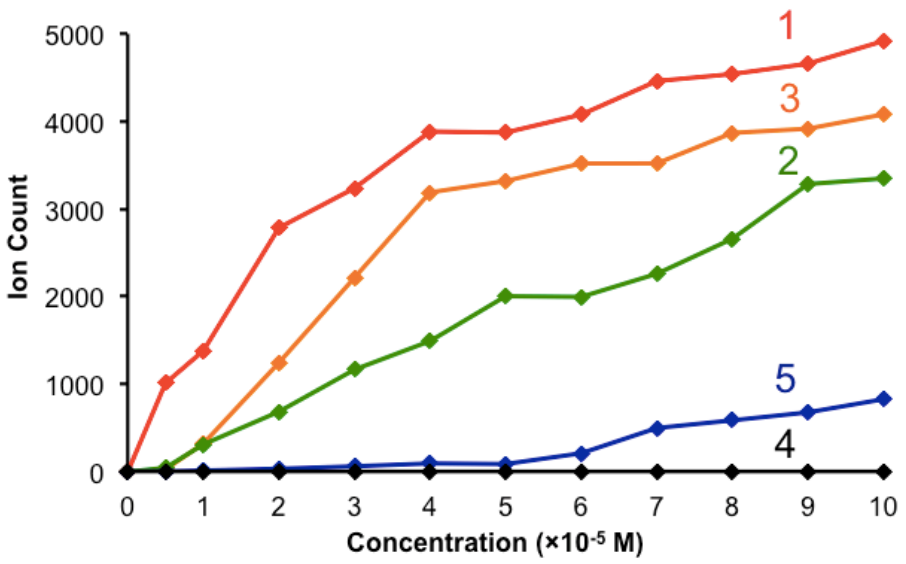

Figure 2.15 – A calibration curve of $[Ph_3C]^+$ with a fixed cone gas flow (50 L/hour), capillary voltage (2750 V), and MCP voltage (2500 V). Each colour represents a different probe position.

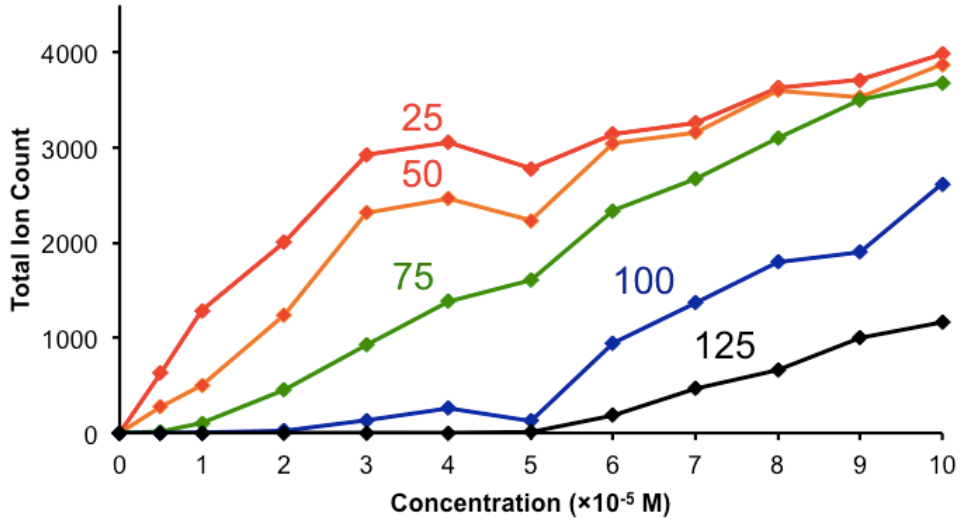

Figure 2.16 – A calibration curve of $[Ph_3C]^+$ with a fixed probe position (2), capillary voltage (2750 V), and MCP voltage (2500 V). Each colour represents a different cone gas flow.

2.6 – Discussion

Calibration curves of de-tuning different instrumental parameters were plotted. Within the concentration range from 10 to 100µmol/L, accurate quantification of different species can, therefore, be determined. Below is an example of overcoming the saturation issue with newly adjusted parameters (Figure 2.17).

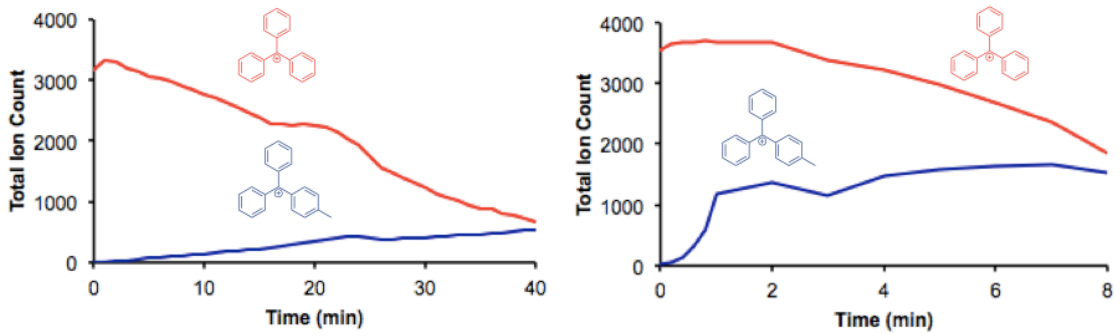

Figure 2.17 – Trimethylaluminum addition to $[Ph_3C]^+$ (left) non-saturated setting of parameters (right) saturated.

An example of performing a reaction under saturated conditions and non-saturated conditions are compared. With optimal settings combined, reaction traces that indicate the appearance of the product and the disappearance of the reactant can be more accurately quantified. More examples of reactions performed under saturated and non-saturated conditions will be described in detail in the following chapter with trialkylaluminum additions to trityl carbocation.

Chapter 3 – Formation and reactivity of $[AlMe_2]^+$

3.1 – Introduction

Group 13 compounds such as methylaluminoxane (MAO)[56], trialkylaluminums[14] (R_3Al), and trityl tetrakis(pentafluorophenyl)borate ($[Ph_3C]^+[B(C_6F_5)_4]^-$)[57] play important roles as activators of olefin polymerization catalysts. Their reactivity with group IV metallocenes as well as their capability of generating a highly active, single-site olefin polymerization catalysts[58] are widely used in industrial applications (Scheme 3.1).

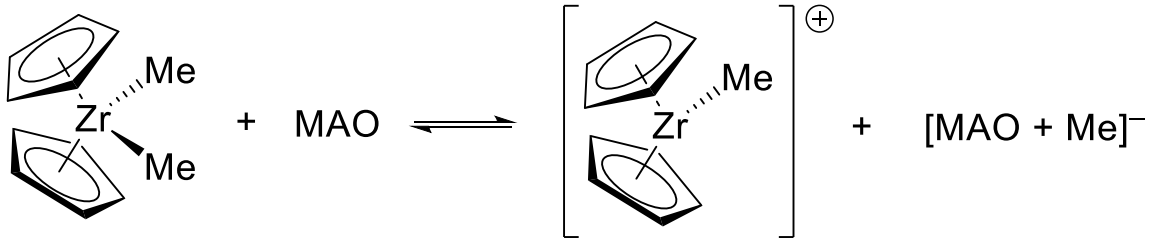

Scheme 3.1 – Activation of single-site olefin polymerization with MAO/zirconocene.

The composition of MAO includes excess Me_3Al due to its partial hydrolytic synthetic route. The excess trimethylaluminum can inhibit the catalytic performance of MAO/metallocene complexes.[18] The role of trimethylaluminum as a reducing agent can facilitate the formation of dinuclear transition metal complexes: this causes the complex to be less catalytically active.[59] Metallocenes as methyl-bridged homobimetallic dinuclear complexes are known as inactive catalysts, as the formation of oligomers rather than high molecular weight polymers are observed[60]. Various approaches have been reported in an effort to reduce the amount of excess trimethylaluminum in MAO via a nonhydrolytic[61]

synthetic route or to remove the excess of trimethylaluminum through evaporation.[62] An alternative to this approach is to prepare aluminoxanate ions. Upon the addition of a Lewis basic mono- or bidentate ligand, for example, octamethyltrisiloxane (OMTS), a stabilized dimethylaluminum cation complex can be synthesized (Scheme 3.2).[34]

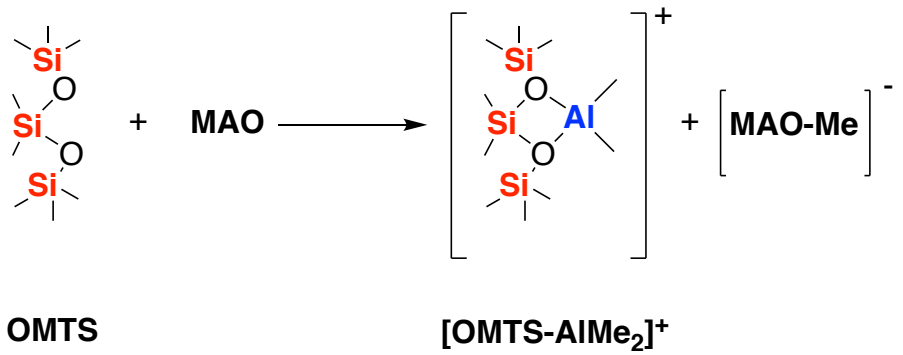

Scheme 3.2 – OMTS addition to MAO.

The activation of a metallocene catalyst with MAO can be performed with the donor-stabilized dimethylaluminum cation. Upon the addition of a dimethylaluminum cation, zirconocene ($(C_5H_5)_2ZrMe_2$) will readily form an ion pair thus generating a $((C_5H_5)_2Zr(\mu\text{-}Me)_2AlMe_2)$ with $[Me\text{-}MAO]^-$ as the counter-anion (Scheme 3.3).[63]

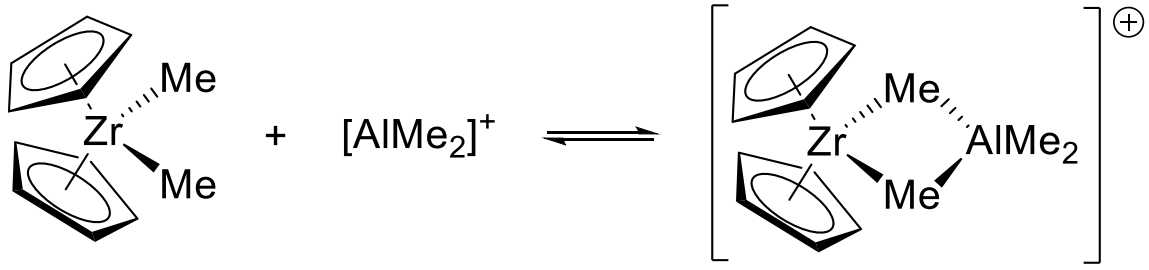

Scheme 3.3 – Catalyst Activation of metallocene with the reactive building block of MAO, $[AlMe_2]^+$.

One disadvantage of the system is the requirement of a high Al/Zr ratio: up to a 5000:1 ratio. As a result, the industry seeks to alleviate these costs through the study of MAO. As the reactivity of MAO relies principally on the $[Me_2Al]^+$ cation, one approach is to emphasize the reactive component: synthesis of the $[Me_2Al]^+$ cation can be performed using trimethylaluminum as suggested in Scheme 3.3. Experiments with ESI-MS have demonstrated the highly reactive nature of the dimethylaluminum cation. In order to avoid any side reactions, it is necessary to stabilize the cation with a donor (Figure 3.4).

$$[Ph_3C]^+[B(C_6F_5)_4]^- \xrightarrow[\text{donor}]{Me_3Al} [Me_2Al\text{-donor}]^+[B(C_6F_5)_4]^-$$

Scheme 3.4 – The formation of a donor-stabilized alumocenium borate complexes.

A donor-stabilized dimethylaluminum cation that requires a lower Al/Zr ratio is an optimal and economical alternative to the MAO/metallocene system. Aside from octamethyltrisiloxane, monodentate Lewis base ligands such as diethyl ether (Et_2O) and tetrahydrofuran (THF) can be used. Reactions where the formation of donor-stabilized alumocenium complexes can be initiated by adding trimethyaluminum to trityl tetrakis(pentafluorophenyl)borate; this is illustrated in Scheme 3.4. The reaction scheme has proved to be effective, as the impressive cocatalytic behaviour can be seen in ethylene-1-octene polymerization from previously reported literature.[34]

3.1.1 Demethylation of Trimethylaluminum and $-CH_2$ addition to trityl

The demethylation of trimethylaluminum accompanied by a reaction demonstrating a $-CH_2$ addition on the phenyl ring, where a methyl addition and a hydride abstraction of the

trityl carbocation was first discovered while approaching the reaction monitoring with a donor-stabilized reaction. This discovery has not been reported before. Bochmann[29] has shown methyl abstraction from Me_3Al by the trityl cation $[Ph_3C]^+$ to form triphenylethane and $[Me_2Al]^+$ (Scheme 3.5). No other reactions were observed aside from the demethylation reaction of trimethylaluminum accompanied by the methylation of the carbocation centre of $[Ph_3C]^+$.[29] From the experimental results, however, inspecting the same reaction by ESI-MS revealed a previously undetected side reaction: the formation of charged species with $-CH_2$ additions to the phenyl ring (Scheme 3.6). Evidence for the +14 Da addition being CH_2 came from high resolution mass spectrometry to establish *m/z*, isotope pattern, MS/MS, and ^1H NMR.

The effect of stoichiometry, the identity of an alkyl group, the sample injection flow rate and the choice of solvent are all factors that can significantly affect the outcome of a reaction. In order to have a better understanding of the reactivity, experiments with varying the parameters are described and the resultant outcomes are compared.

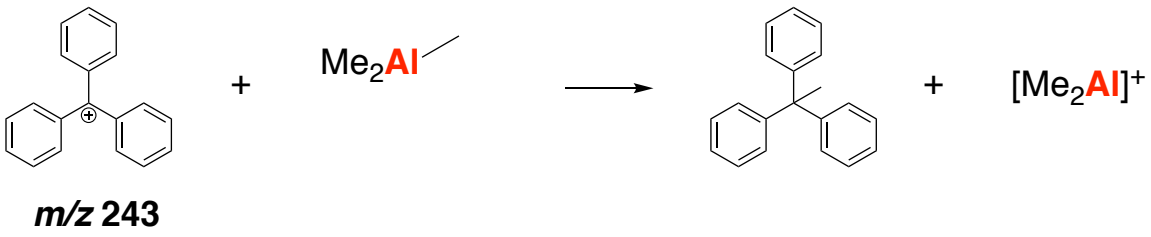

Scheme 3.5 – Literature report of methyl addition of the carbocation centre.[29]

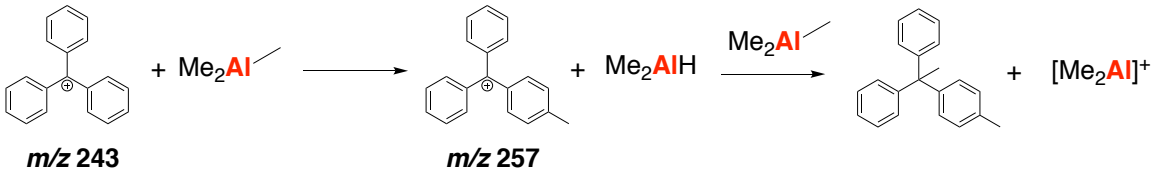

Scheme 3.6 – Reaction scheme for competitive reaction of trimethylaluminum addition.

3.1.2 Tandem Mass Spectrometry (MS/MS)

Tandem mass spectrometry is another powerful tool in mass spectrometry, which allows for a better understanding of the structural information of the analyte. The peak with a *m/z* 257 was selected and a high cone voltage creates fragmentation. The ESI-MS/MS results agree with the assignment: where the data shows the fragmentation of a methylated phenyl ring as a loss of benzene (*m/z* 78) and toluene (*m/z* 92) (Figure 3.1).

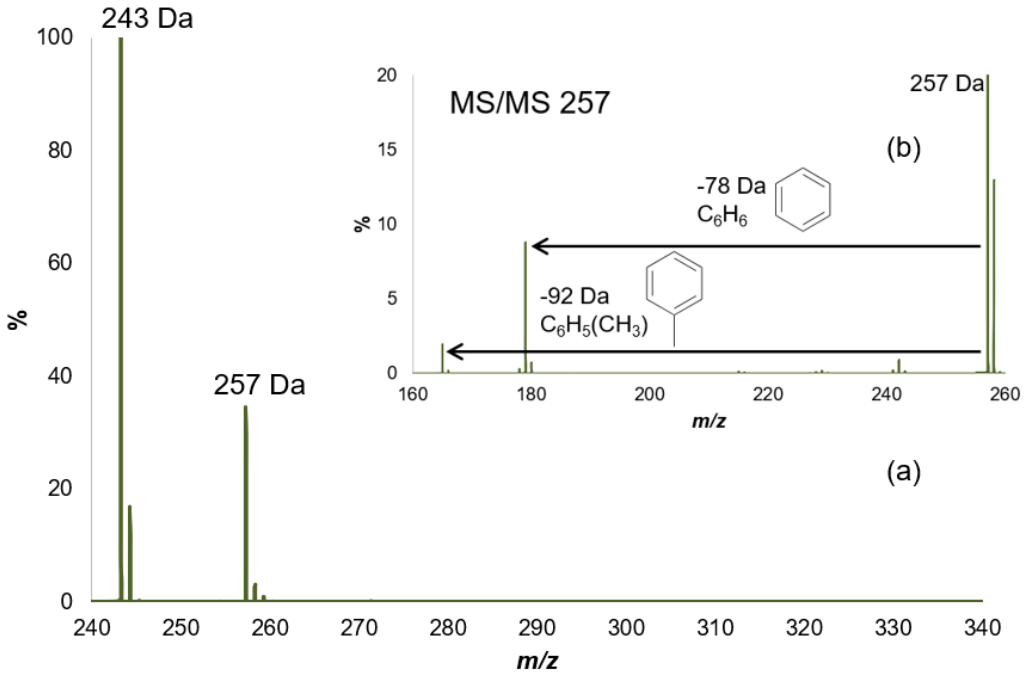

Figure 3.1 – ESI-MS/MS of the ion peak at *m/z* 257. The fragmentation of a C_6H_6 (*m/z* 78) and $C_6H_5(CH_3)$ (*m/z* 92) confirms the identity of the $–CH_2$ addition of $[Ph_3C]^+$.

3.2 – Solvent Effect

A suitable solvent is crucial for sample analysis with ESI-MS.[64] In order to facilitate a practical analysis of the sample, it is ideal to select a solvent with a decent solubility; this facilitates sample preparation, as a solution phase is readily generated, and ionization of droplets could take place.

Table 3.1 tabulates some solvents that are typically used for ESI-MS experiments. The polarity of solvents can be roughly estimated by its dielectric constants. Less polar solvents do not facilitate the required electrochemistry to generate gas phase ions that enable analysis.[65] The lack of conductivity of less polar solvents[66] restricts the process of ions being discharged at the capillary tip.[4] On the other hand, polar solvents are able to solvate and stabilize electrolytes due to the presence of an electric field.[67] The surface tension and the high boiling point are some drawbacks for using water as a solvent in ESI-MS despite its high polarity.[68] To avoid such harsh conditions, other solvents such as methanol, acetonitrile, and dichloromethane with lower surface tensions and boiling points are usually used as alternatives.

Solvents that perform well in synthetic reactions are sometimes not ESI-MS friendly. A successful characterization with ESI-MS is often accompanied by a good choice of solvent as it the quality of electrospray heavily depends on it.[69] Finding a solvent that is suitable for ESI-MS analysis often requires a more careful consideration especially when samples with highly reactive nature are being analyzed. An issue that could arise due to the polarity of the solvent is the coordinating ability where solvents can be further classified as protic or aprotic.[70] For analyses of moisture- and air-sensitive samples, solvents need to be deoxygenated and protic solvents should be avoided.[71]

A nonreactive yet polar solvent is required due to the highly reactive nature of trityl cation, $[Ph_3C]^+$, and trimethylaluminum. The solvent of choice shows drastic differences in the product yield[72] and the reaction rate[73] of trimethylaluminum-related reactions. Relative to solvents such as methanol (ε=33.00) and dichloromethane (ε=8.93), Comparing to other commonly used solvents in ESI-MS from Table 3.1, fluorobenzene and toluene could be classified as much less polar solvents. Nonetheless, due to its non-reactive nature with the sample and the ability to generate a good electrospray, both have been the solvent of choice to investigate the reactivity of trityl carbocation and trimethylaluminum.

One notable variable in mass spectrometric experiments regarding different solvents is the spray quality of the ionization source. The spray quality in electrospray ionization is affected mainly by the polarity of the solvent. Despite various attempts, no stable spray was observed when analyte was prepared in toluene. In order to improve the quality of spray, a minimum ratio, a 75:25 ratio of fluorobenzene/toluene is required (Figure 3.3).

The solvent effect on the reactivity of trityl carbocation to trimethylaluminum can be noted by the spray quality, the reaction rate, and the product yield. A higher ratio of fluorobenzene (Figure 3.2) results in a better spray quality and a faster reaction rate.

Water	80.10	Fluorobenzene	5.47
Acetonitrile	36.64	Toluene	2.38
Methanol	33.00	Benzene	2.28
Dichloromethane	8.93	Hexane	1.89

Table 3.1 – Common solvents and the dielectric constants[74]

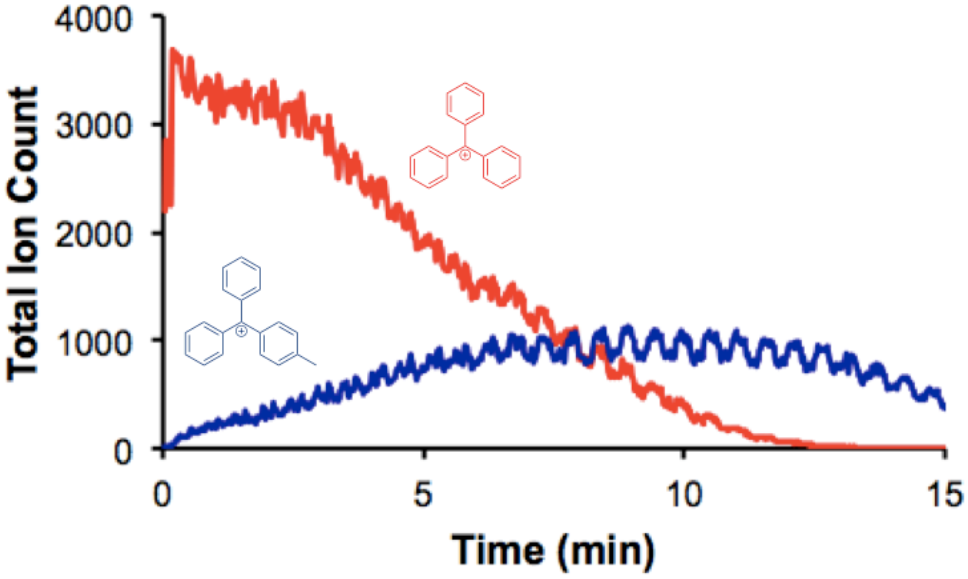

Figure 3.2 – Addition of 1 molar equivalence of Me_3Al to $[Ph_3C]^+$ in fluorobenzene. Capillary voltage held at 3000 V, MCP Detector voltage held at 2700 V, probe position held at 2, and cone gas flow held at 50 L/hour.

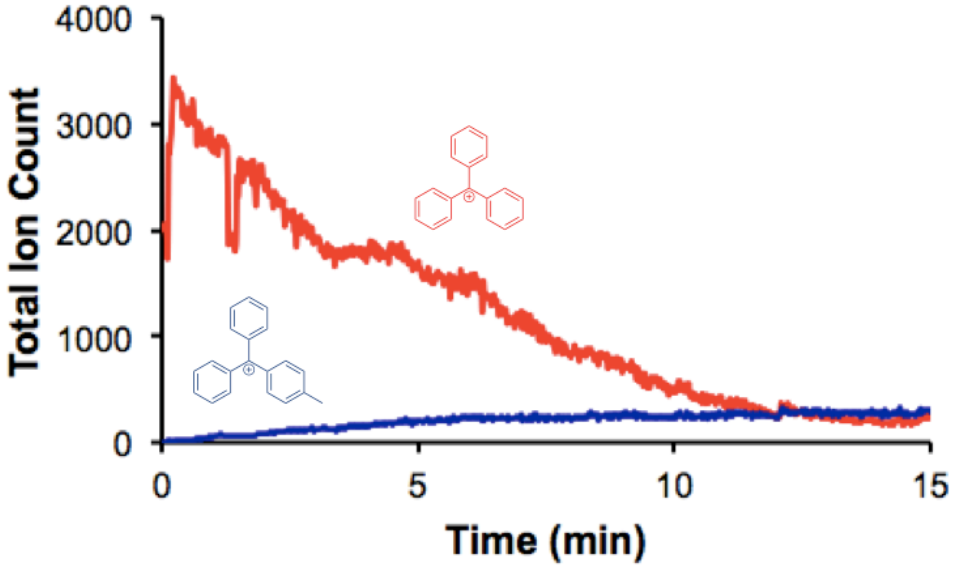

Figure 3.3 – Addition of 1 molar equivalence of Me_3Al to $[Ph_3C]^+$ in 75:25 fluorobenzene/toluene solvent mixture. Capillary voltage held at 3000 V, MCP Detector voltage held at 2700 V, probe position held at 2, and cone gas flow held at 50 L/hour.

3.3 – Flow rate of injection

Prior to analysis with the mass spectrometer, the sample in the solution phase is introduced with a direct sample infusion technique. Despite the facile characterization of ion intensity with ESI-MS, not all the ions are detected with the same efficiency.[75]

Significant effects on the ion count of the instrument can be seen from the sample concentration, the diameter of the metal capillary, and the flow rate.[76] The capillary voltage and the probe positions are the two parameters that have been investigated in the previous chapter. Another important factor that requires attention is the setting of the flow rate on the syringe pump. By varying the liquid flow rate, the formation of the droplet size and the spray quality can be substantially affected.[77]

The flow rate of sample injection is typically reported in the literature where mass spectrometry is used as a characterization technique. In a liquid chromatography-electrospray ionization-mass spectrometry (LC-ESI-MS), selecting an optimal flow rate is crucial to reduce the matrix effect, as an accurate quantification with mass spectrometry can be significantly affected.[78] Nano-electrosprays with a flow rate range from one to a hundred nanoliter per minute has seen increased sensitivity compared to conventional electrospray with a flow rate greater than 1 μL/min.[79] The improvement in sensitivity is likely due to the increased ionization efficiency from the smaller charged droplets generated.[80]

Optimization of sensitivity by lowering the flow rate of injection is however does not solve all issues. From experimental results, the flow rate is also closely associated with the quality of traces seen on a mass spectrum. Combining an optimal concentration with an optimal flow rate is crucial to avoid ion suppression in ESI-MS.[81] Here the effect of flow rate, 20 µL/min (Figure 3.4), 30 µL/min (Figure 3.5), and 40 µL/min (Figure 3.6) on total ion count is reported.

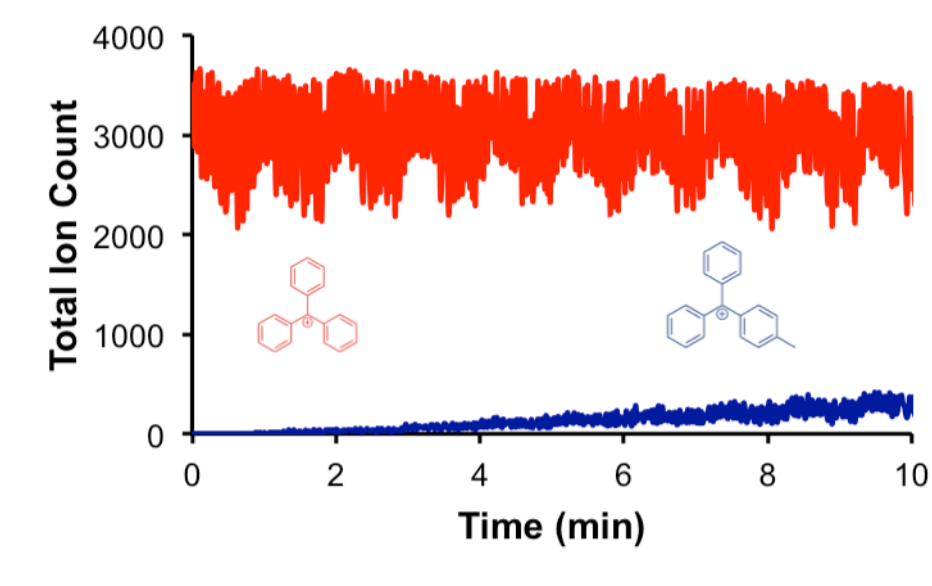

Figure 3.4 – One molar equivalence of trimethylaluminum addition to $[Ph_3C]^+$ with a flow rate at 20 µL/min. Capillary voltage held at 3000 V, MCP Detector voltage held at 2700 V, probe position held at 2, and cone gas flow held at 50 L/hour.

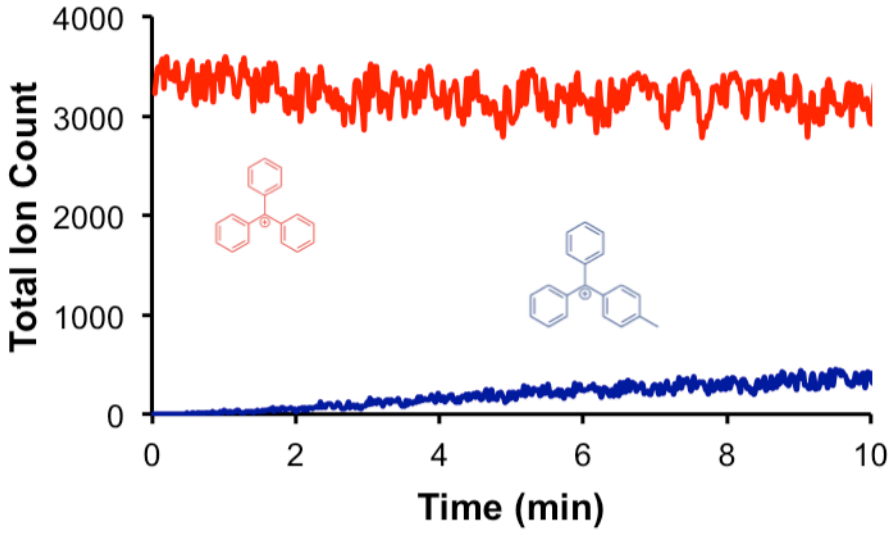

Figure 3.5 – One molar equivalence of trimethylaluminum addition to $[Ph_3C]^+$ with a flow rate at 30 µL/min. Capillary voltage held at 3000 V, MCP Detector voltage held at 2700 V, probe position held at 2, and cone gas flow held at 50 L/hour.

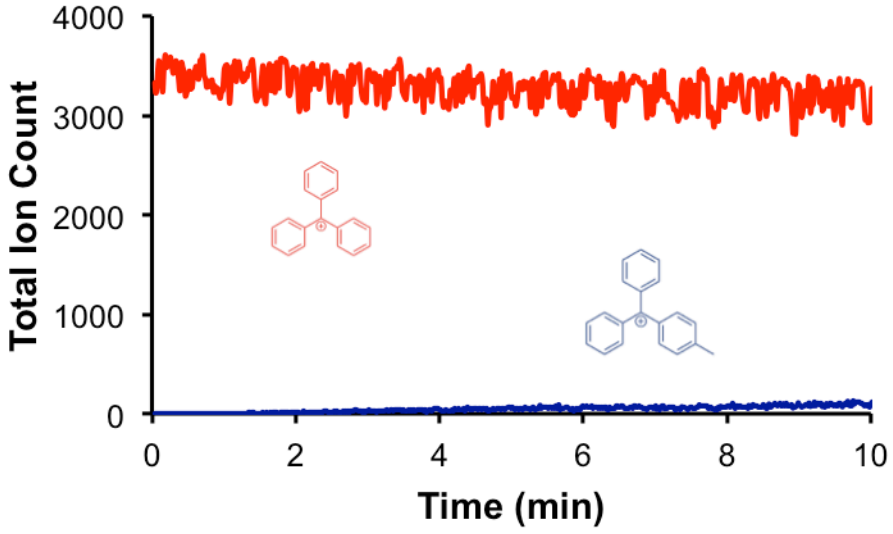

Figure 3.6 – One molar equivalence of trimethylaluminum addition to $[Ph_3C]^+$ with a flow rate at 40 µL/min. Capillary voltage held at 3000 V, MCP Detector voltage held at 2700 V, probe position held at 2, and cone gas flow held at 50 L/hour.

The flow rate of a syringe pump has a significant effect on the quality of the reaction traces. By increasing the flow rate, traces appear to be less noisy. Here three different flow rates were compared and the higher the flow rate allows a better quality of the traces.

3.4 – Other Trialkylaluminums

The reactivity of trityl carbocation, $[Ph_3C]^+$, to trimethylaluminum, Me_3Al, has been investigated with ESI-MS. Aside from previously examined effects on the flow rate and choice of solvent, different choices of trialkylaluminums could result in a different rate of de-alkylation.

The catalytic activity of MAO/metallocene is greatly affected by the amount of excess trimethylaluminum (Me_3Al) as its reducing nature results in the formation of oligomers rather than higher polymers.[14] There is previous literature that reports the effect on the rate of polymerization, the selectivity, and the activity of the catalyst depending on the choices of trialkylaluminums.[82]. By simply substituting triisobutylaluminum (iBu$_3$Al) to trimethylaluminum (Me_3Al), the productivity of each reagent sees a different outcome due to the different preferential reaction mechanisms with metallocenes possessing different isotacticity.[83] A more efficient olefin polymerization has been reported where a trialkylaluminum with a longer chain length yields a better product yield, as for propene polymerization in a MAO/metallocene system, trioctylaluminum (Oct_3Al) demonstrates a higher conversion rate than trimethylaluminum (Me_3Al).[84]

Despite having a similar composition, AlR_3 (where R represents an alkyl chain), the effect of different alkyl chain length results in different reactivity with trityl carbocation. A significant difference in the conversion rate of styrene[85] and ethylene[86] polymerization can be observed as the nature of different trialkylaluminums affects the polymerization conditions.

In this chapter, aside from trimethylaluminum, three other trialkylaluminums, triethy-, triisobtyl-, and trioctyl are the examples to be investigated. Compositional changes that are directly happening to the trityl carbocation can be easily detected in the positive ion mode in electrospray ionization mass spectrometry. The rate and the quantity of de-alkylation from the trialkylaluminums can also be investigated (Figure 3.7).

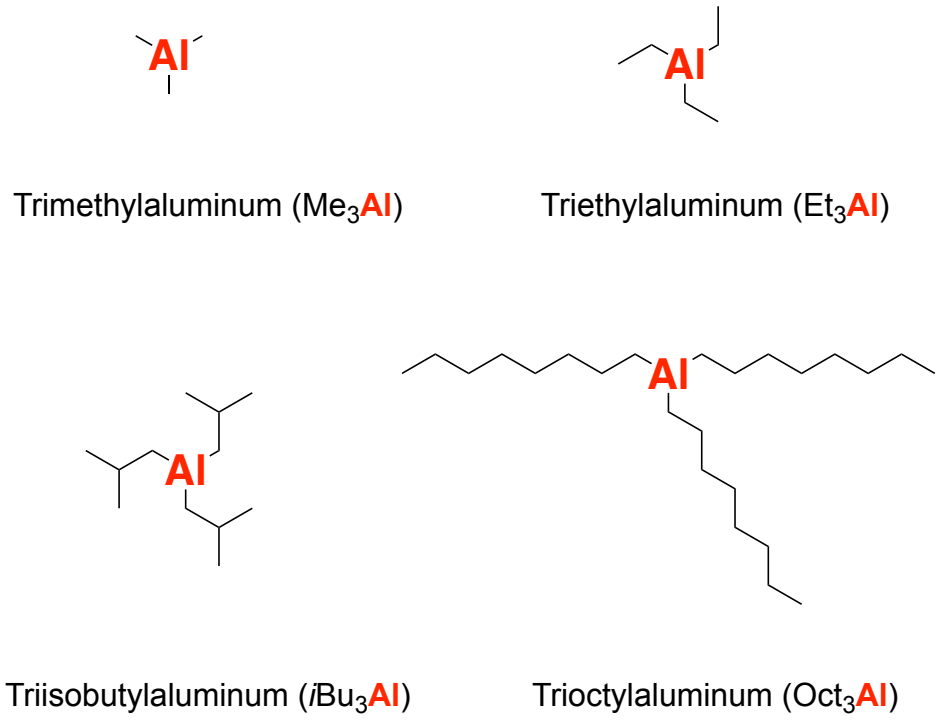

Figure 3.7 – Choices of trialkylalumiums of different chain length investigated.

The reaction scheme of the de-alkylation of the four different trialkylaluminums were investigated (Scheme 3.8). Experimental results of the addition of one molar equivalence of trimethyl- (Figure 3.8), trieethyl (Figure 3.9), triisobutyl (Figure 3.10), and triocylaluminum (Figure 3.11) were plotted. As observed in the intensity in the total ion count comparing two different species, the rate of de-alkylation, the removal of an alkyl group can be seen most effective in triethylaluminum, followed by trioctylaluminum, trimethylaluminum, and triisobutylaluminum.

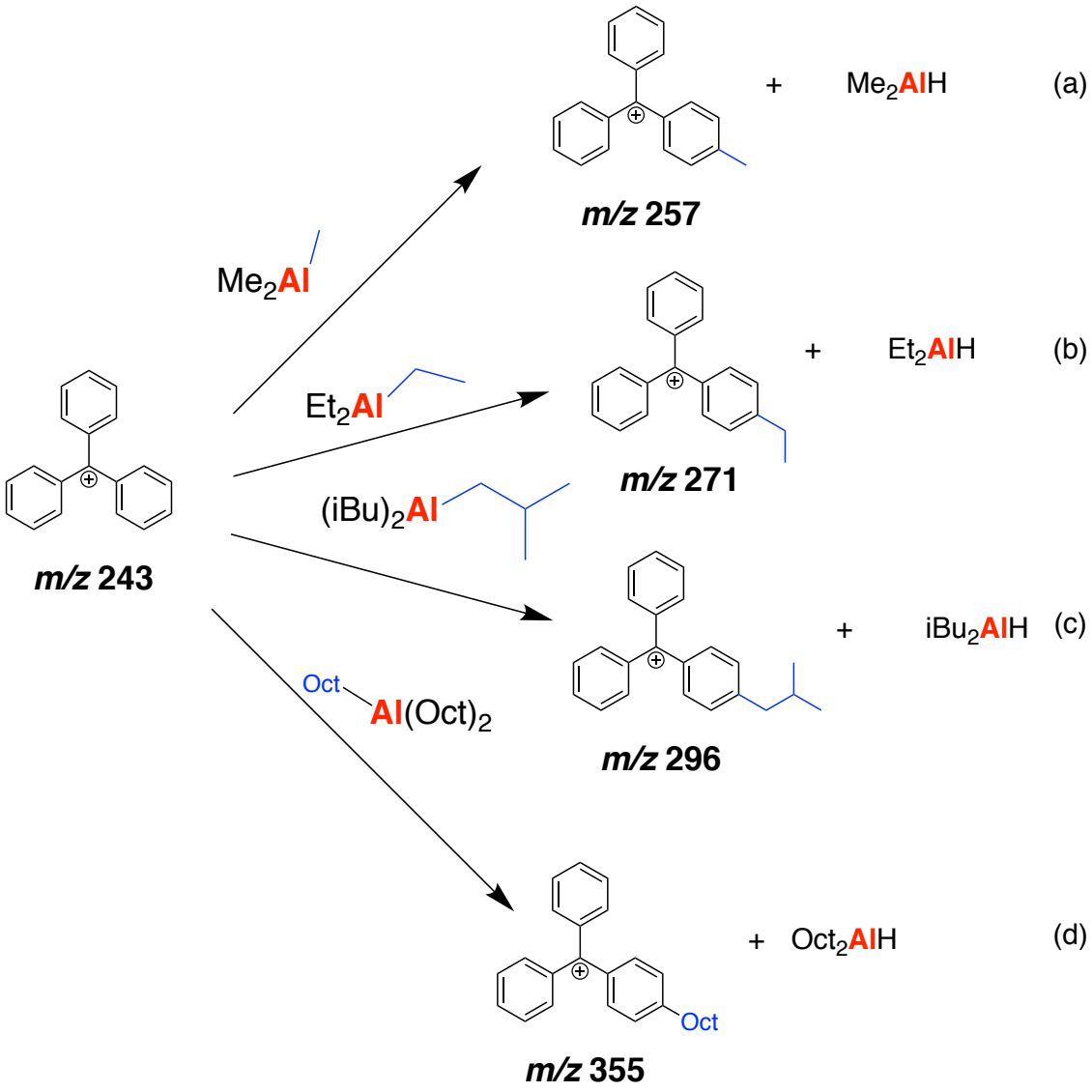

Scheme 3.7 – Reaction scheme of the addition of four different trialkylaluminums to trityl carbocation, $[Ph_3C]^+$. (a)Trimethylaluminum. (b)Triethylaluminum. (c)Triisobutylaluminum. (d) Trioctylaluminum.

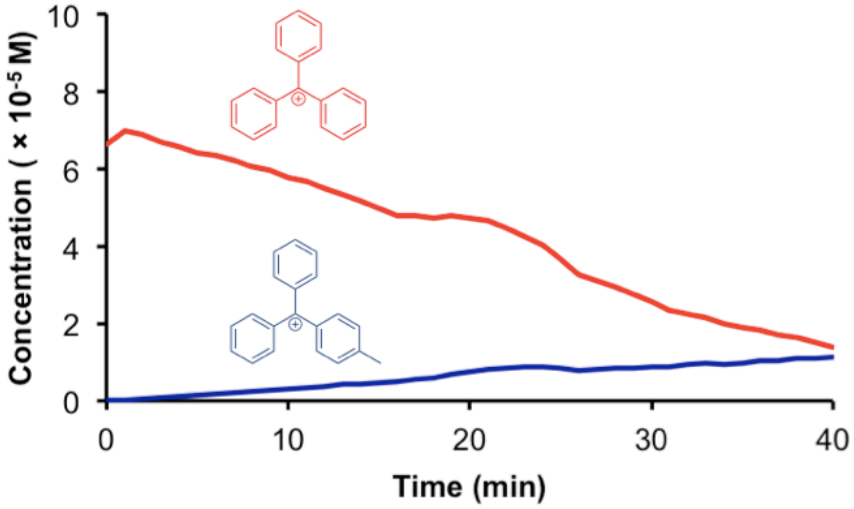

Figure 3.8 – Reaction traces of one molar equivalence of trimethylaluminum addition in fluorobenzene. Capillary voltage held at 2750 V, MCP Detector voltage held at 2500 V, probe position held at 2, and cone gas flow held at 50 L/hour.

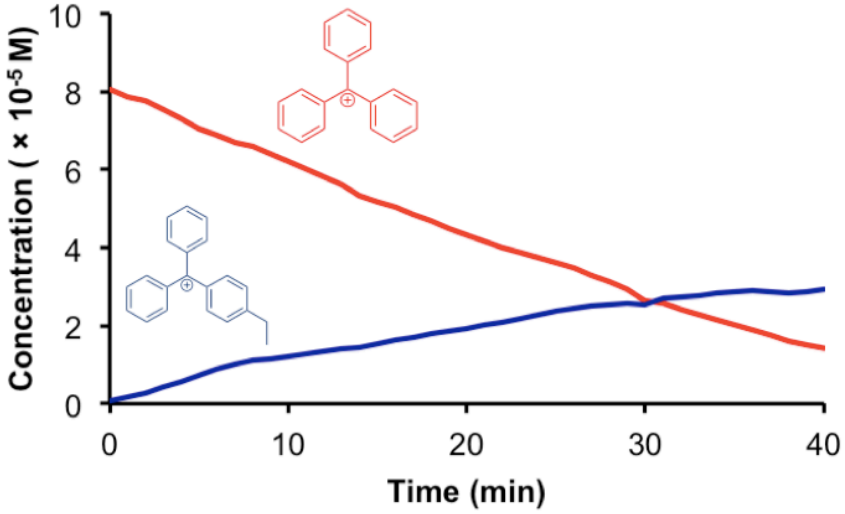

Figure 3.9 – Reaction traces of one molar equivalence of triethylaluminum addition in fluorobenzene. Capillary voltage held at 2750 V, MCP Detector voltage held at 2500 V, probe position held at 2, and cone gas flow held at 50 L/hour.

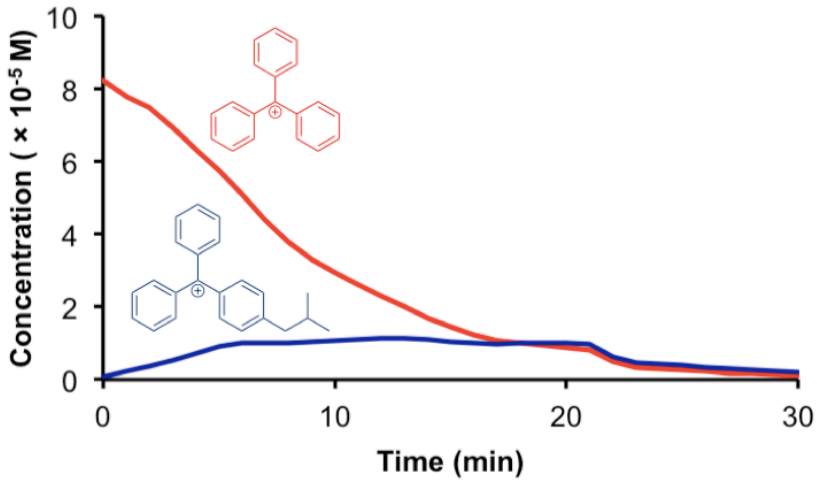

Figure 3.10 – Reaction traces of one molar equivalence of triisobutylaluminum addition in fluorobenzene. Capillary voltage held at 2750 V, MCP Detector voltage held at 2500 V, probe position held at 2, and cone gas flow held at 50 L/hour.

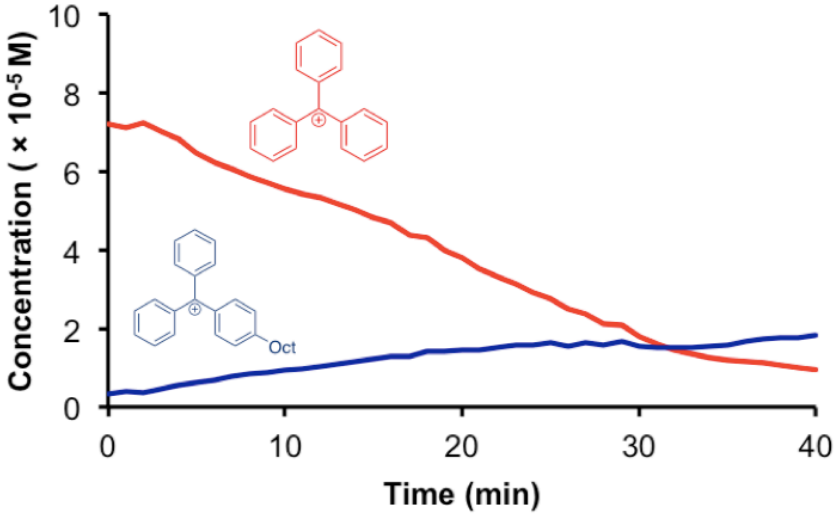

Figure 3.11 – Reaction traces of one molar equivalence of trioctylaluminum addition in fluorobenzene. Capillary voltage held at 2750 V, MCP Detector voltage held at 2500 V, probe position held at 2, and cone gas flow held at 50 L/hour.

3.5 –The discovery of saturation

Change in peak in proton NMR spectrum is a strong evidence of the previously encountered saturation issue as seen from ESI-MS. The quantity of the –CH_2 addition onto the phenyl ring upon the addition of trimethylaluminum can be seen (Figure 3.12). As suggested from the spectrum, the signal intensity of benzylic –C*H* (δ=2-3 ppm) and alkyl –C*H* (δ=1-2 ppm) that show the evidences of the –CH_2 addition onto the phenyl ring were not as abundant as the aromatic –C*H* (δ=6.5-7.5 ppm). This shows the significance of finding the optimal setting that best reflects the true ion count with ESI-MS. The same trend can be seen upon the addition of triethyl- (Figure 3.13), triisobutyl- (Figure 3.14), and trioctylaluminum (Figure 3.15).

3.5.1 Trimethylaluminum

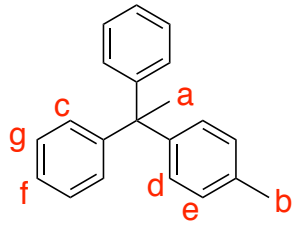

^{1}H NMR (C_6D_6): δ (ppm) 7.28 (t, C*H*-g); 6.96 (t, C*H*-f); 6.88 (d, C*H*-e); 6.76 (d, C*H*-d); 6.67 (d, C*H*-c); 2.02 (s, CH_3-b); 1.37 (s, CH_3-a).

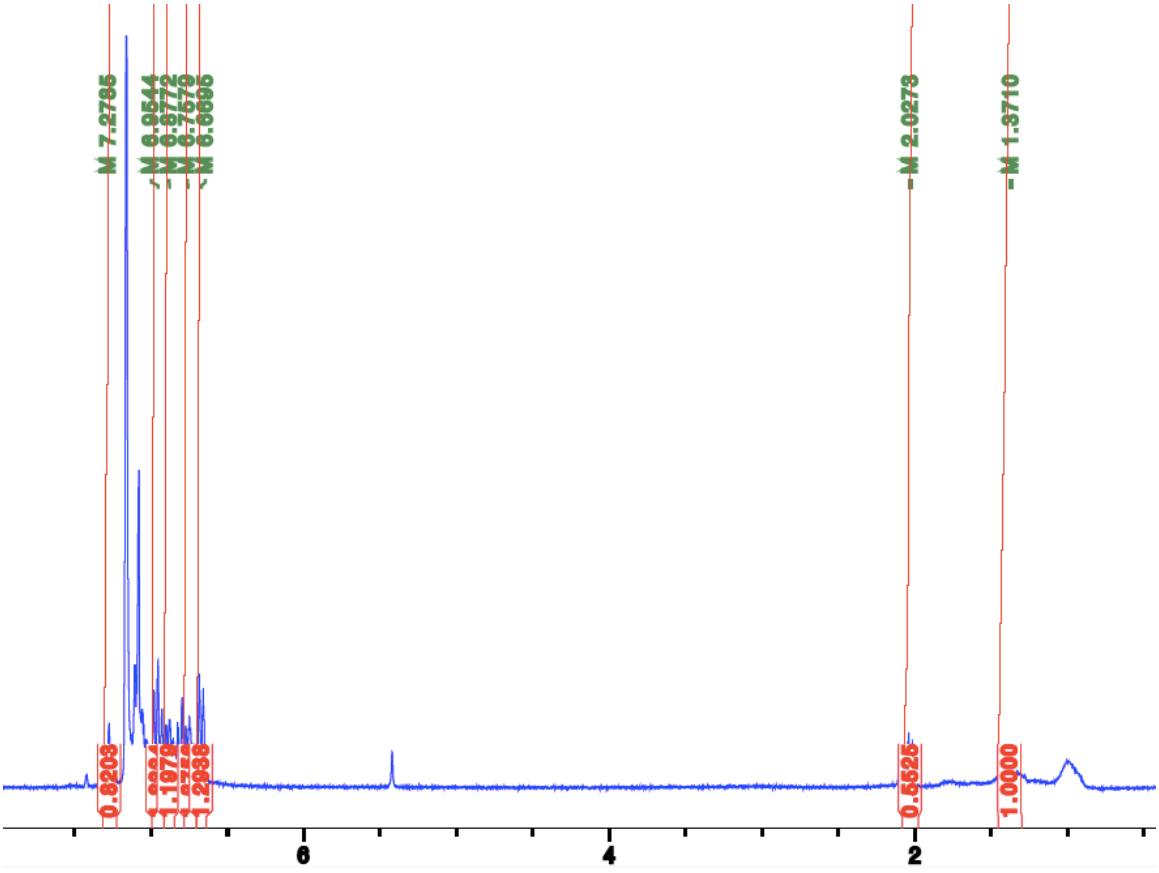

Figure 3.12 – ^{1}HNMR spectrum of one molar equivalence addition of trimethylaluminum to trityl.

3.5.2 Triethylaluminum

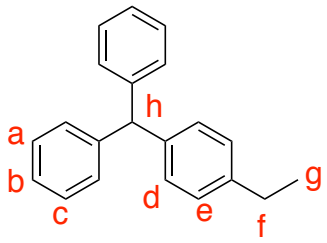

^{1}H NMR (C_6D_6): δ (ppm) 7.23 (t, C*H*-b); 6.94 (t, C*H*-c); 6.89 (d, C*H*-e); 6.80 (d, C*H*-d); 6.59 (d, C*H*-a); 5.42 (s, C*H*-h); 2.13 (m, CH_3-f); 0.80 (t, CH_3-g)

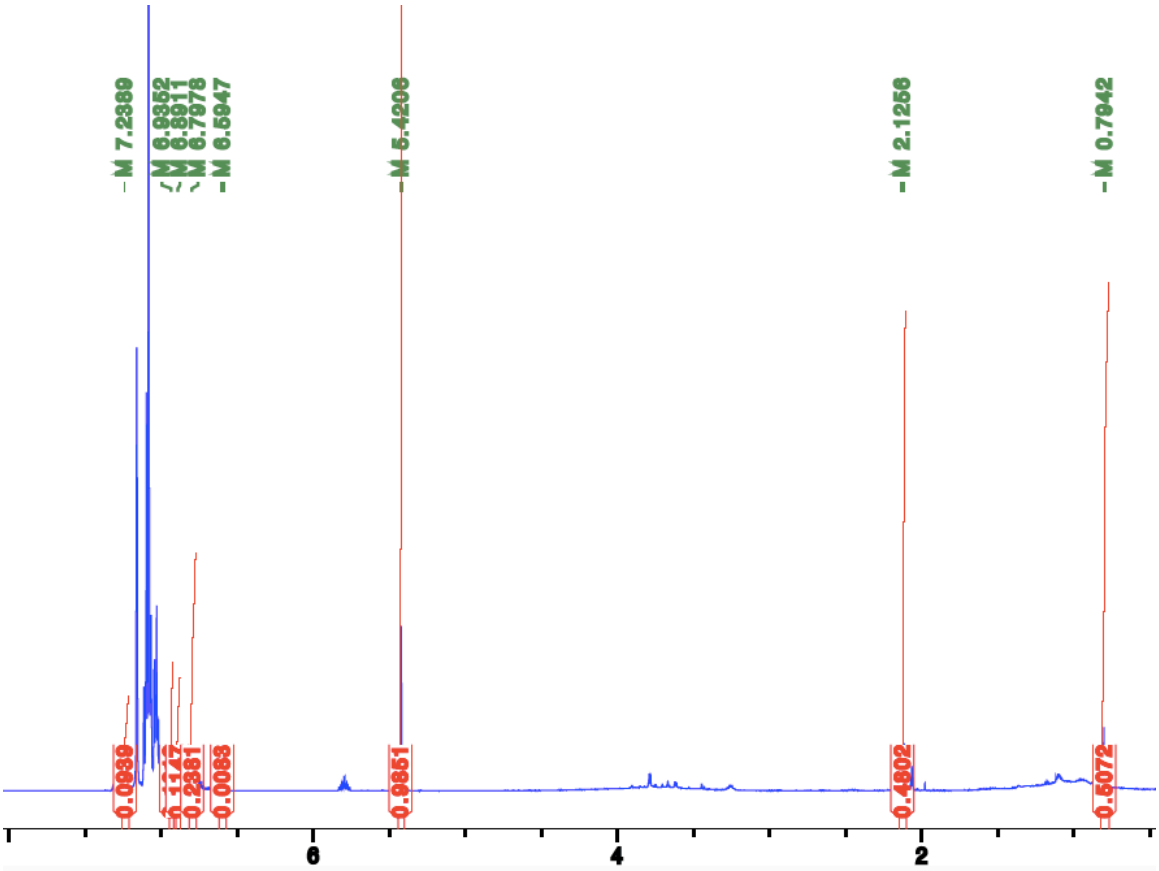

Figure 3.13 – ^{1}H NMR spectrum of one molar equivalence addition of triethylaluminum to trityl.

3.5.3 Triisobutylaluminum

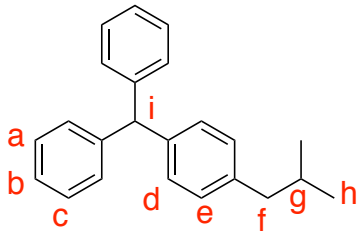

^{1}H NMR (C_6D_6): δ (ppm) 7.37 (t, C*H*-b); 6.81 (t, C*H*-c); 6.75 (d, C*H*-e); 6.65 (d, C*H*-d); 6.48 (d, C*H*-a); 5.41 (s, C*H*-i); 2.19 (m, CH_3-f); 1.25 (m, CH_3-g); 0.92 (d, CH_3-h).

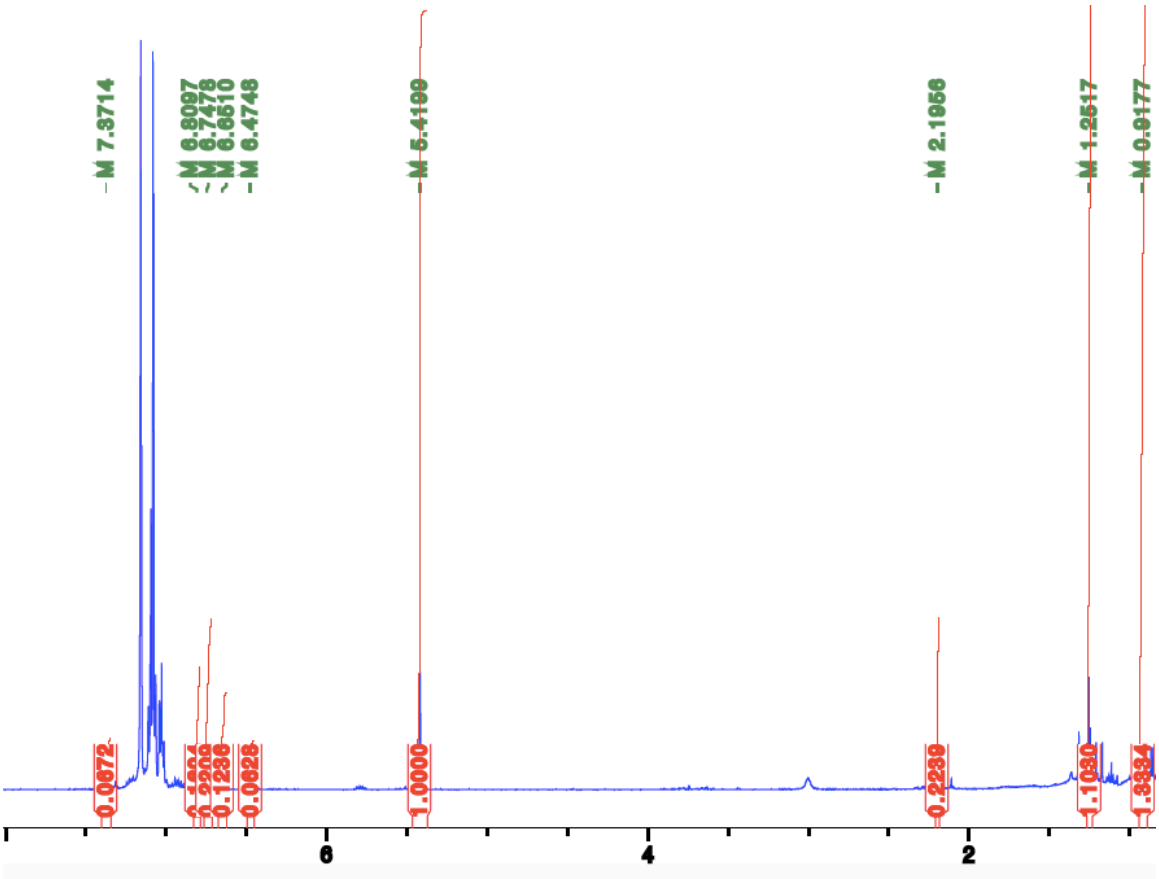

Figure 3.14 – ^{1}H NMR spectrum of one molar equivalence addition of triisobutylaluminum to trityl.

3.5.4 Trioctylaluminum

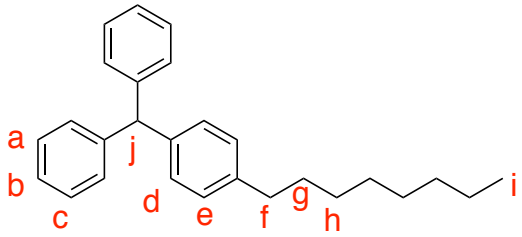

^{1}H NMR (C_6D_6): δ (ppm) 7.23 (t, C*H*-b); 6.92 (t, C*H*-c); 6.88 (d, C*H*-e); 6.82 (d, C*H*-d); 6.65 (d, C*H*-a); 5.41 (s, C*H*-j); 1.90 (t, CH_3-f); 1.47 (t, CH_3-h); 1.08 (m, CH_3-g); 0.72 (t, CH_3-i).

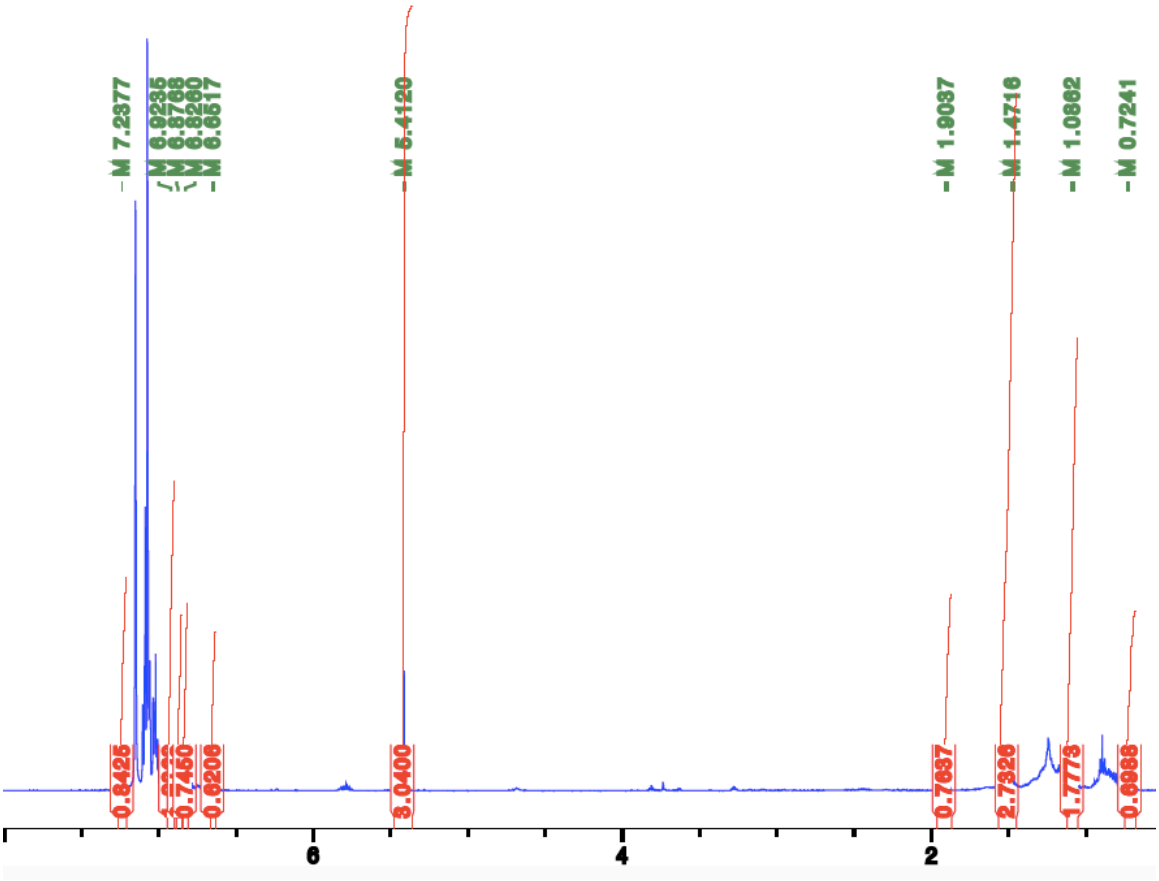

Figure 3.15 – ^{1}H NMR spectrum of one molar equivalence addition of trioctylaluminum to trityl.

3.6 – Overcoming saturation in quantification

Experimental results with ESI-MS show a new type of reactivity of trityl carbocation towards trialkylaluminums. The results, however, indicate saturation, as the reactant and product traces do not correlate to each other, causing an over-representation of the product trace and an under-representation of reactant trace.

From the previous chapter, the optimal combination of settings was discovered regarding the capillary voltage, MCP detector voltage, probe position, and cone gas. Linearity on the calibration curve can be generated within the concentration range as the settings of the instrument were optimized. With the optimal setting of parameters sorted out, we can be confident regarding the quantitative study of the reactivity. In Figure 3.16, a comparison between a spectrum acquired before and after overcoming the saturation condition is illustrated.

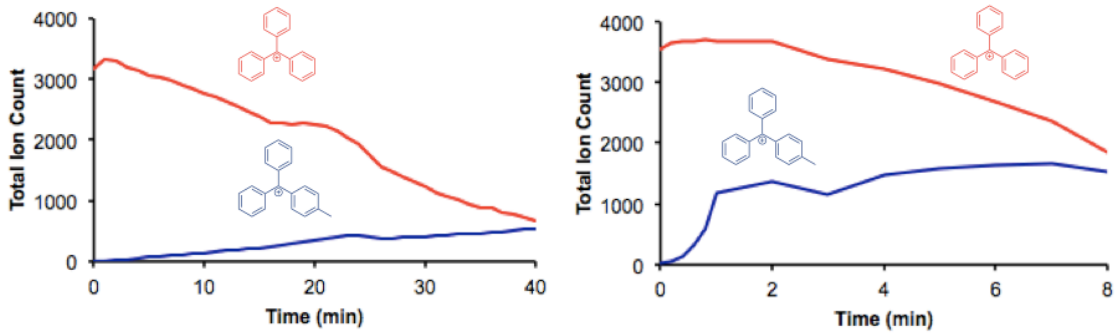

Figure 3.16 – ESI-MS (+) of one molar equivalence of trimethylaluminum addition to $[Ph_3C]^+$ (left) non-saturated (right) saturated in fluorobenzene.

The different quantity of ions can be observed when comparing the saturated and non-saturated spectra of the addition of triethylaluminum (Figure 3.17), triisobutylaluminum (Figure 3.18), and trioctylaluminum (Figure 3.19).

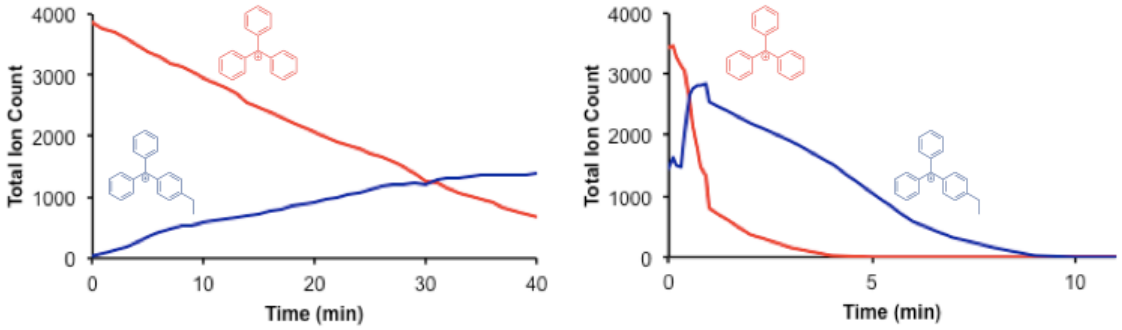

Figure 3.17 – ESI-MS (+) of one molar equivalence of triethylaluminum addition to $[Ph_3C]^+$ (left) non-saturated (right) saturated in fluorobenzene.

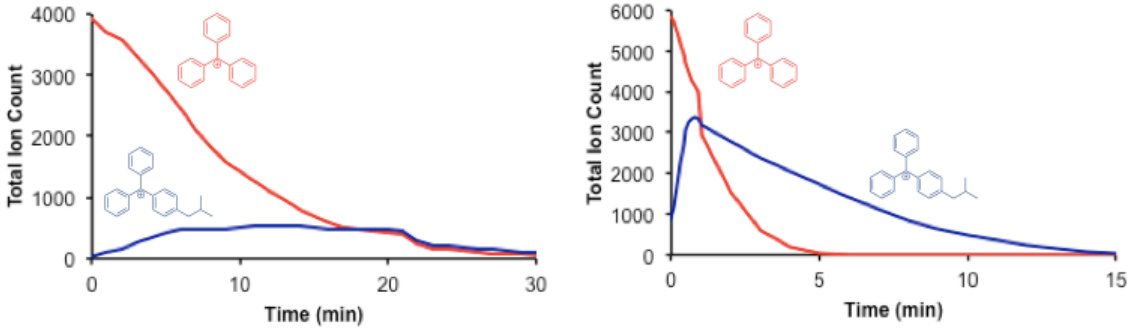

Figure 3.18 – ESI-MS (+) of one molar equivalence of triisobutylaluminum addition to $[Ph_3C]^+$ (left) non-saturated (right) saturated in fluorobenzene.

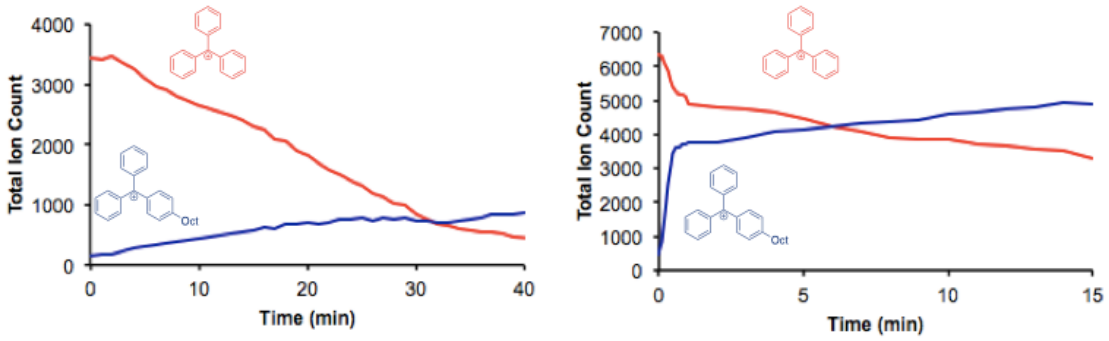

Figure 3.19 – ESI-MS(+) of one molar equivalence of trioctylaluminum addition to $[Ph_3C]^+$ (left) non-saturated (right) saturated in fluorobenzene.

Comparing the saturated and the non-saturated spectra, it can be seen that the spectra before applying the optimal setting do not reflect the true ion count. With the new set of parameters that effectively overcome the saturation issue, a new set of data that truly corresponds to the reactivity between the two species were shown.

3.7 – Stoichiometric effect

As mentioned previously, the Al/Zr ratio was an important factor regarding the catalyst activity in a MAO/metallocene system. In an ethylene homopolymerization reaction, a surprising difference in catalytic activity was observed with a small difference in molar equivalence additions of trialkylaluminums.[87] To study the stoichiometric effect of the de-alkylation of trimethyl- (Figure 3.20), triethyl- (Figure 3.21), triisobutyl- (Figure 3.22), and trioctylaluminum (Figure 3.23) and the reaction rate, experimental results of a one and five molar equivalences of trialkylaluminums addition to $[Ph_3C]^+$ was compared. In the previous chapter, optimal combination of instrumental parameters can be found at setting the capillary voltage at 2700 V, probe position at position 2, MCP detector voltage

at 2500 V, and a cone gas flow at 50 L/hour. Experiments with the addition of all trialkylaluminums are molar equivalences were conducted with above-mentioned conditions. With the optimal settings, accurate quantification was acquired.

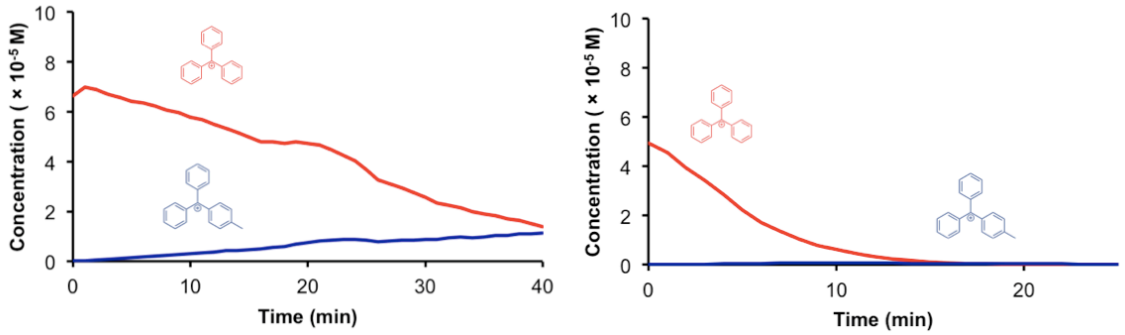

Figure 3.20 – ESI-MS(+) of the addition of trimethylaluminum (left) 1 equivalence (right) 5 equivalences in fluorobenzene. Capillary voltage held at 2750 V, MCP Detector voltage held at 2500 V, probe position held at 2, and cone gas flow held at 50 L/hour.

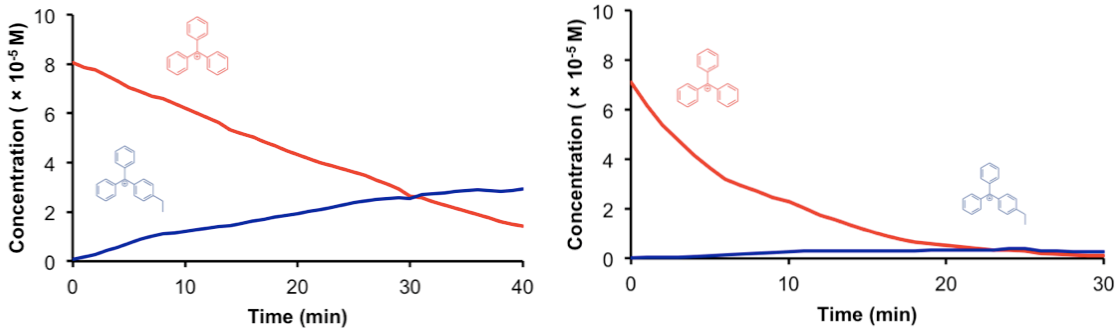

Figure 3.21 – ESI-MS(+) of the addition of triethylaluminum (left) 1 equivalence (right) 5 equivalences in fluorobenzene. Capillary voltage held at 2750 V, MCP Detector voltage held at 2500 V, probe position held at 2, and cone gas flow held at 50 L/hour.

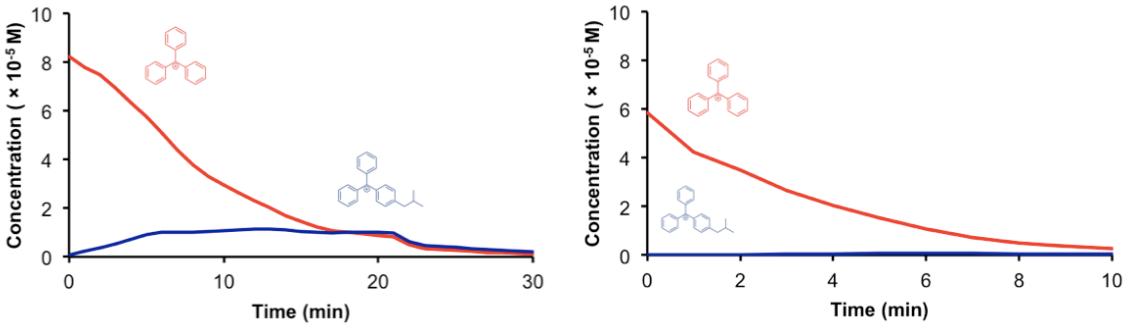

Figure 3.22 – ESI-MS(+) of the addition of triisobutylaluminum (left) 1 equivalence (right) 5 equivalences in fluorobenzene. Capillary voltage held at 2750 V, MCP Detector voltage held at 2500 V, probe position held at 2, and cone gas flow held at 50 L/hour.

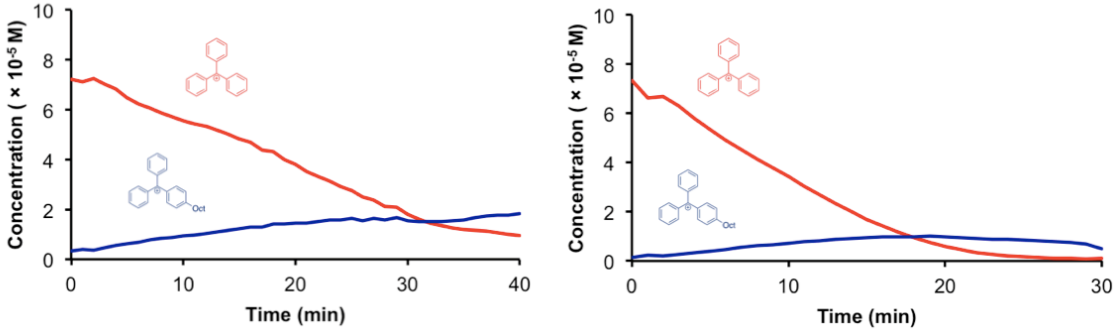

Figure 3.23 – ESI-MS(+) of the addition of trioctylaluminum (left) 1 equivalence (right) 5 equivalences in fluorobenzene. Capillary voltage held at 2750 V, MCP Detector voltage held at 2500 V, probe position held at 2, and cone gas flow held at 50 L/hour.

Experimental results obtained from different trialkylaluminums showed the different rate of de-alkylation upon addition of different trialkylaluminums. Following a similar trend, a higher molar equivalence addition of trioctyl- and triethylaluminum showed a faster de-alkylation rate compared to trimethyl- and triisobutylaluminum. Another notable difference comparing the one to five molar equivalences of addition was the quantity. Upon the addition of five molar equivalences of trialkylaluminums, not only did the

detected quantity of trityl carbocation disappear faster, but the blue traces indicating the product formation also started disappearing just minutes after the formation.

3.8 – Experimental

3.8.1 Sample Preparation

The solvent was dried with calcium hydride overnight, and distillation was performed under an inert nitrogen atmosphere to ensure the absence of moisture in the solvent. The distilled solvent was then stored with activated molecular sieves in the glovebox to avoid contact with moisture and oxygen to ensure optimal experimental conditions.

3.8.2 Material Preparation

A vacuum oven was used for removing traces of moisture. PTFE tubing, sample vials, and syringe that were used to perform the experiment were dried in a vacuum oven for three hours prior to the beginning of the experiment then brought directly into the glovebox for storage.

3.8.3 Addressing Air Sensitivity

An experimental setup such as preparation of the sample and reactions were conducted in a glovebox under the inert nitrogen atmosphere. The sample was introduced directly via a syringe pump, through a drilled hole on the wall of the glovebox into the mass spectrometer. Prior to mass spectrometric experiments, rinsing with solvent was necessary as the residue or contaminants from previous reactions could be cleared to avoid any side reaction.

3.8.4 Data Acquisition

Trityl tetrakis(pentafluorophenyl)borate, $[Ph_3C]^+[B(C_6F_5)_4]^-$, and trialkylaluminum (trimethylaluminum, triethylaluminum, triisobutylaluminum, and trioctylaluminum) were mixed in a sample vial. The reaction mixture of each additional experiment was first

mixed in a sample vial. The sample was then immediately introduced directly into the mass spectrometer with a 1 mL syringe, and an ESI-MS(+) spectrum was recorded. The flow rate was monitored and set up to the 40 μL/min for the acquiring of data unless specified otherwise. A 1 mL syringe was used, and a syringe pump with a constant rate was used.

Chapter 4 – Conclusion

Mass spectrometric studies of highly reactive samples that require a higher concentration often result in saturation. Experimental detuning to lower the sensitivity and data processing with a focus on examining only those parts of the spectrum where saturation is not problematic are the strategies employed to effectively overcome the saturation issue. Trityl carbocation, $[Ph_3C]^+$, is a highly reactive compound that was examined. With an optimal combination of instrumental parameters, a linear calibration curve was generated within the concentration range where both the decomposition and the saturation issues were effectively resolved. Effective instrumental detuning on the capillary voltage, the probe position, the MCP detector voltage, and the cone gas flow, strategies to defeat the saturation can, therefore, broaden of the scope of mass spectrometric studies of more reactive compounds. Future direction of this study could be to investigate the effect of detuning different parameters that were not previously investigated, as this could shine a new light on the understanding of the instrumental response and the effect on sensitivity of ESI-MS. Applying the optimal combination of settings allows accurate quantification studies that are not only limited to trityl carbocation reactivity.

The reactivity of trityl with trialkylaluminums, R_3Al, and the effect of stoichiometry were investigated. Upon addition, a de-alkylation reaction of the trialkylaluminum and an alkyl addition onto the phenyl ring of trityl carbocation were discovered. With a newly discovered reaction, a better understanding regarding the activation chemistry of the MAO-related catalytic activity can be obtained. Experiments with a wider variety of

trialkylaluminums and optimization of the product yield could be the future direction of this study.

Bibliography

(1) Lacorte, S.; Fernandez-Alba, A. R. Time of Flight Mass Spectrometry Applied to the Liquid Chromatographic Analysis of Pesticides in Water and Food. *Mass Spectrom. Rev.* **2006**. https://doi.org/10.1002/mas.20094.

(2) Wilm, M. Principles of Electrospray Ionization. *Mol. Cell. Proteomics* **2011**. https://doi.org/10.1074/mcp.m111.009407.

(3) Fenn, J. B.; Mann, M.; Meng, C. K.; Wong, S. F.; Whitehouse, C. M. Electrospray Ionization–Principles and Practice. *Mass Spectrom. Rev.* **1990**. https://doi.org/10.1002/mas.1280090103.

(4) Kebarle, P. A Brief Overview of the Present Status of the Mechanisms Involved in Electrospray Mass Spectrometry. *Journal of Mass Spectrometry*. 2000. https://doi.org/10.1002/1096-9888(200007)35:7<804::AID-JMS22>3.0.CO;2-Q.

(5) Kebarle, P.; Verkcerk, U. H. Electrospray: From Ions in Solution to Ions in the Gas Phase, What We Know Now. *Mass Spectrom. Rev.* **2009**. https://doi.org/10.1002/mas.20247.

(6) CS Ho, CWK Lam*, MHM Chan, RCK Cheung, LK Law, LCW Lit, KF Ng, MWM Suen, and H. T. Electrospray Ionisation Mass Spectrometry: Principles and Clinical Applications. *Clin Biochem Rev* **2003**. https://doi.org/10.1146/annurev.bi.64.070195.001531.

(7) Traeger, J. C. Electrospray Mass Spectrometry of Organometallic Compounds. *Int. J. Mass Spectrom.* **2000**. https://doi.org/10.1016/S1387-3806(00)00346-8.

(8) Cech, N. B.; Enke, C. G. Practical Implications of Some Recent Studies in

Electrospray Ionization Fundamentals. *Mass Spectrom. Rev.* **2001**. https://doi.org/10.1002/mas.10008.

(9) Hermans, J.; Ongay, S.; Markov, V.; Bischoff, R. Physicochemical Parameters Affecting the Electrospray Ionization Efficiency of Amino Acids after Acylation. *Anal. Chem.* **2017**. https://doi.org/10.1021/acs.analchem.7b01899.

(10) Chernushevich, I. V.; Loboda, A. V.; Thomson, B. A. An Introduction to Quadrupole-Time-of-Flight Mass Spectrometry. *J. Mass Spectrom.* **2001**. https://doi.org/10.1002/jms.207.

(11) Douglas, D. J.; French, J. B. Collisional Focusing Effects in Radio Frequency Quadrupoles. *J. Am. Soc. Mass Spectrom.* **1992**. https://doi.org/10.1016/1044-0305(92)87067-9.

(12) El-Aneed, A.; Cohen, A.; Banoub, J. Mass Spectrometry, Review of the Basics: Electrospray, MALDI, and Commonly Used Mass Analyzers. *Applied Spectroscopy Reviews*. 2009. https://doi.org/10.1080/05704920902717872.

(13) Kaminsky, W. Highly Active Metallocene Catalysts for Olefin Polymerization. *Journal of the Chemical Society - Dalton Transactions*. 1998. https://doi.org/10.1039/a800056e.

(14) Chen, E. Y. X.; Marks, T. J. Cocatalysts for Metal-Catalyzed Olefin Polymerization: Activators, Activation Processes, and Structure-Activity Relationships. *Chem. Rev.* **2000**. https://doi.org/10.1021/cr980462j.

(15) Kaminsky, W.; Külper, K.; Brintzinger, H. H.; Wild, F. R. W. P. Polymerization of Propene and Butene with a Chiral Zirconocene and Methylalumoxane as Cocatalyst. *Angew. Chemie Int. Ed. English* **1985**.

https://doi.org/10.1002/anie.198505071.

(16) Kristen, M. O. Supported Metallocene Catalysts with MAO and Boron Activators. *Top. Catal.* **1999**. https://doi.org/10.1023/A:1019195229418.

(17) Bochmann, M. The Chemistry of Catalyst Activation: The Case of Group 4 Polymerization Catalysts. *Organometallics* **2010**. https://doi.org/10.1021/om1004447.

(18) Imhoff, D. W.; Simeral, L. S.; Sangokoya, S. A.; Peel, J. H. Characterization of Methylaluminoxanes and Determination of Trimethylaluminum Using Proton NMR. *Organometallics* **1998**. https://doi.org/10.1021/om980046p.

(19) Tritto, I.; Sacchi, M. C.; Locatelii, P.; Li, S. X. Low-Temperature 1H and 13C NMR Investigation of Trimethylaluminium Contained in Methylaluminoxane Cocatalyst for Metallocene-Based Catalysts in Olefin Polymerization. *Macromol. Chem. Phys.* **1996**. https://doi.org/10.1002/macp.1996.021970429.

(20) Linnolahti, M.; Laine, A.; Pakkanen, T. A. Screening the Thermodynamics of Trimethylaluminum-Hydrolysis Products and Their Co-Catalytic Performance in Olefin-Polymerization Catalysis. *Chem. - A Eur. J.* **2013**. https://doi.org/10.1002/chem.201204450.

(21) Atwood, J. L.; Hrncir, D. C.; Priester, R. D.; Rogers, R. D. Decomposition of High-Oxygen Content Organoaluminum Compounds. The Formation and Structure of the [AI7O6Me16]-Anion. *Organometallics* **1983**. https://doi.org/10.1021/om50002a008.

(22) Mason, M. R.; Barron, A. R.; Smith, J. M.; Bott, S. G. Hydrolysis of Tri-Tert-Butylaluminum: The First Structural Characterization of Alkylalumoxanes

[(R2Al)2O]n and (RAlO)N. *J. Am. Chem. Soc.* **1993**. https://doi.org/10.1021/ja00065a005.

(23) Babushkin, D. E.; Semikolenova, N. V.; Panchenko, V. N.; Sobolev, A. P.; Zakharov, V. A.; Talsi, E. P. Multinuclear NMR Investigation of Methylaluminoxane. *Macromol. Chem. Phys.* **1997**. https://doi.org/10.1002/macp.1997.021981206.

(24) Trefz, T. K.; Henderson, M. A.; Linnolahti, M.; Collins, S.; Scott McIndoe, J. Mass Spectrometric Characterization of Methylaluminoxane-Activated Metallocene Complexes. *Chem. - A Eur. J.* **2015**. https://doi.org/10.1002/chem.201405319.

(25) Ghiotto, F.; Pateraki, C.; Tanskanen, J.; Severn, J. R.; Luehmann, N.; Kusmin, A.; Stellbrink, J.; Linnolahti, M.; Bochmann, M. Probing the Structure of Methylalumoxane (MAO) by a Combined Chemical, Spectroscopic, Neutron Scattering, and Computational Approach. *Organometallics* **2013**. https://doi.org/10.1021/om4002878.

(26) Zijlstra, H. S.; Linnolahti, M.; Collins, S.; McIndoe, J. S. Additive and Aging Effects on Methylalumoxane Oligomers. *Organometallics* **2017**. https://doi.org/10.1021/acs.organomet.7b00153.

(27) Kaminsky, W. How to Reduce the Ratio Mao/Metallocene. *Macromol. Symp.* **1995**. https://doi.org/10.1002/masy.19950970108.

(28) Quevedo-Sanchez, B.; Nimmons, J. F.; Coughlin, E. B.; Henson, M. A. Kinetic Modeling of the Effect of MAO/Zr Ratio and Chain Transfer to Aluminum in Zirconocene Catalyzed Propylene Polymerization. *Macromolecules* **2006**.

https://doi.org/10.1021/ma060880n.

(29) Bochmann, M.; Sarsfield, M. J. Reaction of AlR3 with CPh3 B(C6F5)(4) : Facile Degradation of B(C6F5)(4) (-) by Transient " AlR2 (+)." *Organometallics* **1998**.

(30) Glaser, R.; Sun, X. Thermochemistry of the Initial Steps of Methylaluminoxane Formation. Aluminoxanes and Cycloaluminoxanes by Methane Elimination from Dimethylaluminum Hydroxide and Its Dimeric Aggregates. *J. Am. Chem. Soc.* **2011**. https://doi.org/10.1021/ja109457j.

(31) Chien, J. C. W.; Tsai, W. M.; Rausch, M. D.; Rausch, M. D. Isospecific Polymerization of Propylene Catalyzed by Rac-Ethylenebis(Indenyl)Methylzirconium "Cation." *J. Am. Chem. Soc.* **1991**. https://doi.org/10.1021/ja00022a081.

(32) Pédeutour, J. N.; Radhakrishnan, K.; Cramail, H.; Deffieux, A. Reactivity of Metallocene Catalysts for Olefin Polymerization: Influence of Activator Nature and Structure. *Macromolecular Rapid Communications*. 2001. https://doi.org/10.1002/1521-3927(20011001)22:14<1095::AID-MARC1095>3.0.CO;2-R.

(33) Yang, X.; Stern, C. L.; Marks, T. J. "Cation-like" Homogeneous Olefin Polymerization Catalysts Based upon Zirconocene Alkyls and Tris(Pentafluorophenyl)Borane. *J. Am. Chem. Soc.* **1991**. https://doi.org/10.1021/ja00009a076.

(34) Klosin, J.; Roof, G. R.; Chen, E. Y. X.; Abboud, K. A. Ligand Exchange and Alkyl Abstraction Involving (Perfluoroaryl)Boranes and -Alanes with Aluminum and Gallium Alkyls. *Organometallics* **2000**. https://doi.org/10.1021/om000573k.

(35) Stahl, N. G.; Salata, M. R.; Marks, T. J. B(C6F5)3- vs Al(C6F 5)3-Derived Metallocenium Ion Pairs. Structural, Thermochemical, and Structural Dynamic Divergences. *J. Am. Chem. Soc.* **2005**. https://doi.org/10.1021/ja0429622.

(36) Maurer, M. M.; Donohoe, G. C.; Valentine, S. J. Advances in Ion Mobility-Mass Spectrometry Instrumentation and Techniques for Characterizing Structural Heterogeneity. *Analyst*. 2015. https://doi.org/10.1039/c5an00922g.

(37) PRZYBYLSKI, M.; GLOCKER, M. O. ChemInform Abstract: Electrospray Mass Spectrometry of Biomacromolecular Complexes with Noncovalent Interactions - New Analytical Perspectives for Supramolecular Chemistry and Molecular Recognition Processes. *ChemInform* **2010**. https://doi.org/10.1002/chin.199631320.

(38) Leize, E.; Jaffrezic, A.; Van Dorsselaer, A. Correlation between Solvation Energies and Electrospray Mass Spectrometric Response Factors. Study by Electrospray Mass Spectrometry of Supramolecular Complexes in Thermodynamic Equilibrium in Solution. *J. Mass Spectrom.* **1996**. https://doi.org/10.1002/(SICI)1096-9888(199605)31:5<537::AID-JMS330>3.0.CO;2-M.

(39) Agnes, G. R.; Horlick, G. Electrospray Mass Spectrometry as a Technique for Elemental Analysis: Quantitative Aspects. *Appl. Spectrosc.* **2005**. https://doi.org/10.1366/000370294774368875.

(40) Ikonoraou, M. G.; Blades, A. T.; Kebarle, P. Investigations of the Electrospray Interface for Liquid Chromatography/Mass Spectrometry. *Anal. Chem.* **1990**. https://doi.org/10.1021/ac00208a012.

(41) Volmer, D. A.; Jessome, L. L. Ion Suppression: A Major Concern in Mass Spectrometry. *LCGC North Am.* **2006**.

(42) Janusson, E.; Hesketh, A. V.; Bamford, K. L.; Hatlelid, K.; Higgins, R.; McIndoe, J. S. Spatial Effects on Electrospray Ionization Response. *Int. J. Mass Spectrom.* **2015**. https://doi.org/10.1016/j.ijms.2015.07.016.

(43) Ramaley, L.; Herrera, L. C. Software for the Calculation of Isotope Patterns in Tandem Mass Spectrometry. *Rapid Commun. Mass Spectrom.* **2008**. https://doi.org/10.1002/rcm.3668.

(44) Hanlan, J.; Skoog, D. A.; West, D. M. Principles of Instrumental Analysis. *Stud. Conserv.* **2006**. https://doi.org/10.2307/1505543.

(45) Treutler, H.; Neumann, S. Prediction, Detection, and Validation of Isotope Clusters in Mass Spectrometry Data. *Metabolites* **2016**. https://doi.org/10.3390/metabo6040037.

(46) Tang, L.; Kebarle, P. Dependence of Ion Intensity in Electrospray Mass Spectrometry on the Concentration of the Analytes in the Electrosprayed Solution. *Anal. Chem.* **1993**. https://doi.org/10.1021/ac00072a020.

(47) Benkestock, K.; Sundqvist, G.; Edlund, P. O.; Roeraade, J. Influence of Droplet Size, Capillary-Cone Distance and Selected Instrumental Parameters for the Analysis of Noncovalent Protein-Ligand Complexes by Nano-Electrospray Ionization Mass Spectrometry. *J. Mass Spectrom.* **2004**. https://doi.org/10.1002/jms.685.

(48) Cox, J. T.; Marginean, I.; Smith, R. D.; Tang, K. On the Ionization and Ion Transmission Efficiencies of Different ESI-MS Interfaces. *J. Am. Soc. Mass*

Spectrom. **2014**. https://doi.org/10.1007/s13361-014-0998-5.

(49) Agnes, G. R.; Horlick, G. Determination of Solution Ions by Electrospray Mass Spectrometry. *Appl. Spectrosc.* **2005**. https://doi.org/10.1366/000370294774368965.

(50) Tang, L.; Kebarle, P. Spectrometry on the Concentration of the Analytes in The. *Anal. Chem.* **1993**.

(51) Bilbao, A.; Gibbons, B. C.; Slysz, G. W.; Crowell, K. L.; Monroe, M. E.; Ibrahim, Y. M.; Smith, R. D.; Payne, S. H.; Baker, E. S. An Algorithm to Correct Saturated Mass Spectrometry Ion Abundances for Enhanced Quantitation and Mass Accuracy in Omic Studies. *Int. J. Mass Spectrom.* **2018**. https://doi.org/10.1016/j.ijms.2017.11.003.

(52) Xu, X.; Chen, Y.; Sun, J. Indenyl Abstraction versus Alkyl Abstraction of [(Indenyl)ScR 2(Thf)] by [Ph3C] [B(C6F5) 4]: Aspecific and Syndiospecific Styrene Polymerization. *Chem. - A Eur. J.* **2009**. https://doi.org/10.1002/chem.200802220.

(53) Nogrette, F.; Heurteau, D.; Chang, R.; Bouton, Q.; Westbrook, C. I.; Sellem, R.; Clément, D. Characterization of a Detector Chain Using a FPGA-Based Time-to-Digital Converter to Reconstruct the Three-Dimensional Coordinates of Single Particles at High Flux. *Rev. Sci. Instrum.* **2015**. https://doi.org/10.1063/1.4935474.

(54) Kinsel, G. R.; Preston, L. M.; Russell, D. H. Fragmentation of Vitamin B12 during 337 Nm Matrix-assisted Laser Desorption Ionization. *Biol. Mass Spectrom.* **1994**. https://doi.org/10.1002/bms.1200230404.

(55) Luo, X.; Chen, B.; Ding, L.; Tang, F.; Yao, S. HPLC-ESI-MS Analysis of Vitamin

B12 in Food Products and in Multivitamins-Multimineral Tablets. *Anal. Chim. Acta* **2006**. https://doi.org/10.1016/j.aca.2006.01.073.

(56) Sinn, H.; Kaminsky, W.; Vollmer, H. -J; Woldt, R. "Living Polymers" on Polymerization with Extremely Productive Ziegler Catalysts. *Angew. Chemie Int. Ed. English* **1980**. https://doi.org/10.1002/anie.198003901.

(57) Ewen, J. A. Propylene Polymerizations with Metallocene/Teal/Trityl Tetrakis (Pentafluorophenyl) Aluminate Mixtures. *Stud. Surf. Sci. Catal.* **1994**. https://doi.org/10.1016/S0167-2991(08)63054-2.

(58) Chakraborty, D.; Chen, E. Y.-X. Neutral Olefin Polymerization Activators as Highly Active Catalysts for ROP of Heterocyclic Monomers and for Polymerization of Styrene. *Macromolecules* **2002**. https://doi.org/10.1021/ma011813q.

(59) Hammawa, H.; Mannan, T. M.; Lynch, D. T.; Wanke, S. E. Effects of Aluminum Alkyls on Ethylene/1-Hexene Polymerization with Supported Metallocene/MAO Catalysts in the Gas Phase. *J. Appl. Polym. Sci.* **2004**. https://doi.org/10.1002/app.20396.

(60) Busico, V.; Cipullo, R.; Cutillo, F.; Friederichs, N.; Ronca, S.; Wangt, B. Improving the Performance of Methylalumoxane: A Facile and Efficient Method to Trap "Free" Trimethylaluminum. *J. Am. Chem. Soc.* **2003**. https://doi.org/10.1021/ja0372412.

(61) Obrey, S. J.; Bott, S. G.; Barron, A. R. Aluminum Alkoxides as Synthons for Methylalumoxane (MAO): Product-Catalyzed Thermal Decomposition of [Me2Al(μ-OCPh3)]2. *Organometallics* **2001**. https://doi.org/10.1021/om0106128.

(62) Tian, J.; Hustad, P. D.; Coates, G. W. A New Catalyst for Highly Syndiospecific Living Olefin Polymerization: Homopolymers and Block Copolymers from Ethylene and Propylene. *Journal of the American Chemical Society*. 2001. https://doi.org/10.1021/ja0157189.

(63) Babushkin, D. E.; Brintzinger, H. H. Activation of Dimethyl Zirconocene by Methylaluminoxane (MAO)-Size Estimate for Me-MAO- Anions by Pulsed Field-Gradient NMR. *J. Am. Chem. Soc.* **2002**. https://doi.org/10.1021/ja020646m.

(64) Cole, R. B.; Harrata, A. K. Solvent Effect on Analyte Charge State, Signal Intensity, and Stability in Negative Ion Electrospray Mass Spectrometry; Implications for the Mechanism of Negative Ion Formation. *J. Am. Soc. Mass Spectrom.* **1993**. https://doi.org/10.1016/1044-0305(93)85016-Q.

(65) Henriksen, T.; Juhler, R. K.; Svensmark, B.; Cech, N. B. The Relative Influences of Acidity and Polarity on Responsiveness of Small Organic Molecules to Analysis with Negative Ion Electrospray Ionization Mass Spectrometry (ESI-MS). *J. Am. Soc. Mass Spectrom.* **2005**. https://doi.org/10.1016/j.jasms.2004.11.021.

(66) Henderson, M. A.; McIndoe, J. S. Ionic Liquids Enable Electrospray Ionisation Mass Spectrometry in Hexane. *Chem. Commun.* **2006**. https://doi.org/10.1039/b606938j.

(67) Bruins, A. P. Mechanistic Aspects of Electrospray Ionization. *Journal of Chromatography A*. 1998. https://doi.org/10.1016/S0021-9673(97)01110-2.

(68) Tang, L.; Kebarle, P. Effect of the Conductivity of the Electrosprayed Solution on the Electrospray Current. Factors Determining Analyte Sensitivity in Electrospray Mass Spectrometry. *Anal. Chem.* **1991**. https://doi.org/10.1021/ac00023a009.

(69) Wang, H. Y.; Zhang, J. T.; Zhang, S. S.; Guo, Y. L. The Remarkable Role of Solvent in Reaction Mechanism Studies by Electrospray Mass Spectrometry. *Org. Chem. Front.* **2015**. https://doi.org/10.1039/c5qo00154d.

(70) Huffman, B. A.; Poltash, M. L.; Hughey, C. A. Effect of Polar Protic and Polar Aprotic Solvents on Negative-Ion Electrospray Ionization and Chromatographic Separation of Small Acidic Molecules. *Anal. Chem.* **2012**. https://doi.org/10.1021/ac302397b.

(71) Henderson, W.; McIndoe, J. S. *Mass Spectrometry of Inorganic, Coordination and Organometallic Compounds*; 2005. https://doi.org/10.1002/0470014318.

(72) Muthukumaru Pillai, S.; Tembe, G. L.; Ravindranathan, M.; Sivaram, S. Dimerization of Ethylene to 1-Butene Catalyzed by the Titanium Alkoxide-Trialkylaluminum System. *Ind. Eng. Chem. Res.* **1988**. https://doi.org/10.1021/ie00083a003.

(73) Cornish, A. J.; Läppert, M. F. Homogeneous Catalysis. IX. Hydrosilylation Using Tris(Pentanedionato)Rhodium(III)-Trialkylaluminium as Catalyst. *J. Organomet. Chem.* **1984**. https://doi.org/10.1016/0022-328X(84)85171-2.

(74) Ed, D. R. L.; Lide, D. R. CRC Handbook of Chemistry and Physics, 84th Edition, 2003-2004. *Handb. Chem. Phys.* **2003**. https://doi.org/10.1136/oem.53.7.504.

(75) Koivusalo, M.; Haimi, P.; Heikinheimo, L.; Kostiainen, R.; Somerharju, P. Quantitative Determination of Phospholipid Compositions by ESI-MS: Effects of Acyl Chain Length, Unsaturation, and Lipid Concentration on Instrument Response. *J. Lipid Res.* **2001**.

(76) Juraschek, R.; Röllgen, F. W. Pulsation Phenomena during Electrospray

Ionization. *Int. J. Mass Spectrom.* **1998**. https://doi.org/10.1016/S1387-3806(98)14025-3.

(77) Schmidt, A.; Karas, M.; Dülcks, T. Effect of Different Solution Flow Rates on Analyte Ion Signals in Nano-ESI MS, or: When Does ESI Turn into Nano-ESI? *J. Am. Soc. Mass Spectrom.* **2003**. https://doi.org/10.1016/S1044-0305(03)00128-4.

(78) Kloepfer, A.; Quintana, J. B.; Reemtsma, T. Operational Options to Reduce Matrix Effects in Liquid Chromatography- Electrospray Ionisation-Mass Spectrometry Analysis of Aqueous Environmental Samples. *J. Chromatogr. A* **2005**. https://doi.org/10.1016/j.chroma.2004.11.101.

(79) El-Faramawy, A.; Siu, K. W. M.; Thomson, B. A. Efficiency of Nano-Electrospray Ionization. *J. Am. Soc. Mass Spectrom.* **2005**. https://doi.org/10.1016/j.jasms.2005.06.011.

(80) Wilm, M. S.; Mann, M. Electrospray and Taylor-Cone Theory, Dole's Beam of Macromolecules at Last? *Int. J. Mass Spectrom. Ion Process.* **1994**. https://doi.org/10.1016/0168-1176(94)04024-9.

(81) Tang, K.; Page, J. S.; Smith, R. D. Charge Competition and the Linear Dynamic Range of Detection in Electrospray Ionization Mass Spectrometry. *J. Am. Soc. Mass Spectrom.* **2004**. https://doi.org/10.1016/j.jasms.2004.04.034.

(82) Ribeiro, M. R.; Deffieux, A.; Portela, M. F. Supported Metallocene Complexes for Ethylene and Propylene Polymerizations: Preparation and Activity. *Ind. Eng. Chem. Res.* **1997**. https://doi.org/10.1021/ie960475s.

(83) Maciejewski Petoff, J. L.; Myers, C. L.; Waymouth, R. M. Influence of Trialkylaluminum Reagents on the Propylene Polymerization Behavior of Bridged

and Unbridged 2-Arylindene Metallocene Polymerization Catalysts. *Macromolecules* **1999**. https://doi.org/10.1021/ma990659t.

(84) Shiono, T.; Yoshida, S.; Hagihara, H.; Ikeda, T. Additive Effects of Trialkylaluminum on Propene Polymerization with (t-BuNSiMe2Flu)TiMe2-Based Catalysts. *Appl. Catal. A Gen.* **2000**. https://doi.org/10.1016/S0926-860X(00)00633-5.

(85) Vasilenko, I. V.; Kostjuk, S. V.; Kaputsky, F. N.; Nedorezova, P. M.; Aladyshev, A. M. Effect of Different Aluminum Alkyls on the Metallocene/Methylaluminoxane Catalyzed Polymerization of Higher α-Olefins and Styrene. *Macromol. Chem. Phys.* **2008**. https://doi.org/10.1002/macp.200800024.

(86) de Souza, C. G.; de Souza, R. F.; Bernardo-Gusmão, K. Effect of Alkylaluminum Cocatalyst on Ethylene Polymerization with Nickel-α-Diimine Complex. *Appl. Catal. A Gen.* **2007**. https://doi.org/10.1016/j.apcata.2007.03.007.

(87) Chen, M.; Zou, W.; Cai, Z.; Chen, C. Norbornene Homopolymerization and Copolymerization with Ethylene by Phosphine-Sulfonate Nickel Catalysts. *Polym. Chem.* **2015**. https://doi.org/10.1039/c5py00010f.